nature reviews clean technology

https://doi.org/10.1038/s44359-024-00002-4

Review article

Check for updates

Flash Joule heating for synthesis, upcycling and remediation

Bing Deng[1] ✉, Lucas Eddy[2,3,4], Kevin M. Wyss[5], Chandra Sekhar Tiwary[6] & James M. Tour[3,4,7,8,9] ✉

Abstract

Electric heating methods are being developed and used to electrify industrial applications and lower their carbon emissions. Direct Joule resistive heating is an energy-efficient electric heating technique that has been widely tested at the bench scale and could replace some energy-intensive and carbon-intensive processes. In this Review, we discuss the use of flash Joule heating (FJH) in processes that are traditionally energy-intensive or carbon-intensive. FJH uses pulse current discharge to rapidly heat materials directly to a desired temperature; it has high-temperature capabilities (>3,000 °C), fast heating and cooling rates (>10^2 °C s^{-1}), short duration (milliseconds to seconds) and high energy efficiency (~100%). Carbon materials and metastable inorganic materials can be synthesized using FJH from virgin materials and waste feedstocks. FJH is also applied in resource recovery (such as from e-waste) and waste upcycling. An emerging application is in environmental remediation, where FJH can be used to rapidly degrade perfluoroalkyl and polyfluoroalkyl substances and to remove or immobilize heavy metals in soil and solid wastes. Life-cycle and technoeconomic analyses suggest that FJH can reduce energy consumption and carbon emissions and be cost-efficient compared with existing methods. Bringing FJH to industrially relevant scales requires further equipment and engineering development.

Sections

[1]School of Environment, Tsinghua University, Beijing, China. [2]Applied Physics Program, Rice University, Houston, TX, USA. [3]Department of Chemistry, Rice University, Houston, TX, USA. [4]Smalley-Curl Institute, Rice University, Houston, TX, USA. [5]SLB, Houston, TX, USA. [6]School of Nanoscience and Technology, Indian Institute of Technology, Kharagpur, India. [7]Department of Materials Science and NanoEngineering, Rice University, Houston, TX, USA. [8]NanoCarbon Center, Rice University, Houston, TX, USA. [9]Rice Advanced Materials Institute, Rice University, Houston, TX, USA. ✉e-mail: dengbing@tsinghua.edu.cn; tour@rice.edu

Key points

- Flash Joule heating (FJH) uses pulsed intense electric discharge to rapidly and directly heat materials for a short duration.
- Carbon materials, such as graphene, and inorganic materials can be synthesized using FJH and a variety of feedstocks.
- Waste can be managed and upcycled using FJH techniques, which are more energy efficient than conventional methods such as furnace-based heating.
- Remediation of soil contaminated with heavy metals and organic pollutants is feasible at laboratory scales with FJH.
- Life-cycle assessments suggest that compared with various other synthesis and waste management methods, FJH has reduced energy consumption and carbon emissions, especially when using waste feedstocks; FJH also appears to be cost-effective based on preliminary technoeconomic analyses.
- FJH is largely demonstrated at the bench scale, but scale-up of FJH is now being demonstrated on an industrial scale for materials production.

Introduction

Industrial processes responsible for chemicals and raw materials production frequently demand large quantities of heat for tasks such as steam generation, melting, refining, separation and drying[1]. Currently, much of this industrial heating is powered by coal or natural gas combustion[2] and, in theory, could be replaced by electricity-based heating methods. Therefore, industrial electrification[3] — the transition from fossil fuel-based technologies to electricity-based technologies — is instrumental in decarbonizing society, as the industrial sector contributes ~26% of global carbon emissions[4]. However, industrial electrification is still in early stages and requires technological innovation[5].

Electric heating methods encompass a range of technologies such as resistance heating[6] (Box 1), electric arc heating[7], induction heating[8] and dielectric heating[9]. These methods differ in energy efficiency, temperature range and heating rate, for instance (Supplementary Table 1). Direct electric Joule resistive heating[10] is emerging as a promising heating technique because of its very high energy efficiency (100% electricity-to-heat conversion efficiency), as it involves no intermediate heat transfer. Flash Joule heating (FJH) is a type of direct resistance heating that occurs when a high-power, short-duration electrical pulse from a power source passes through a material, rapidly generating intense heat directly within the chosen material without the need for a heating medium to transfer the heat[11]. The high efficiency, short duration, solvent-free nature and minimal heat loss of FJH processes are improvements compared with other processes such as radiative heating or wet methods[12].

Following its introduction in 2020 for converting carbon sources into high-quality graphene[11], FJH has been scaled, and its applications have expanded. FJH has been used in various materials synthesis and thermal treatment processes (Fig. 1A), including in bottom-up synthesis of graphene[11,13], carbon nanotubes[14], carbides[15], borides[16], nitrides[17], metallic glasses[18,19], transition-metal dichalcogenides and *p*-block metal chalcogenides[20], as well as doped and functionalized variants of these compounds[21]. Waste materials can be used as feedstocks for materials synthesis, providing a substantial reduction in energy intensity and emissions for many FJH processes relative to using virgin materials[12,22]. FJH has also been applied in resource recovery and waste decontamination, including in perfluoroalkyl and polyfluoroalkyl substances (PFAS) destruction[23,24], soil remediation[25], waste plastic upcycling[14,26], and extraction of rare earth metals[27].

In this Review, we describe FJH, covering its fundamental principles, equipment design, applications, industrial implementation, sustainability and technoeconomic considerations (Fig. 1A). We begin by discussing the basic principles and theories underlying FJH, as well as the equipment and reactor designs. Subsequently, we highlight its potential applications in fields such as synthesis of carbon materials and metastable inorganic materials, resource recovery and waste upcycling, and environmental remediation. Sustainability and technoeconomic considerations are further discussed. Finally, we outline the remaining challenges that must be addressed to make FJH a mainstay of manufacturing and environmental stewardship.

Principles, equipment and scalability

In this section, the principles behind FJH are introduced, the apparatus and systems are demonstrated, and various reactor designs targeting different applications are discussed. Next, the ongoing scaling up of the FJH process toward industry-scale implementation is briefly discussed.

Fundamentals

Joule heating is a process by which an electrical current that passes through a resistive medium heats this medium by Joule's law, according to which the heating power is equal to the electrical potential difference times the current flowing through the medium[28]. Here, we define flash Joule heating as a direct heating process with a high-power, short-duration electrical pulse generated by a power source that is applied directly to a resistive material, causing extremely rapid heating of the target material to a wide temperature range, followed by rapid cooling. The target material can itself be the resistive material, or the target material can be in direct contact with the resistive material. The current density can exceed 10 A mm^{-2} and, when used in conjunction with a suitable electrically resistive material, leads to ultrahigh temperatures that can even exceed 3,500 °C (ref. 11). The current pulse width can be as short as milliseconds to seconds, resulting in ultrafast heating rates (typically 10^2 to 10^5 °C s^{-1}; refs. 11,15) and ultrafast cooling rates (typically 10^2 to 10^4 °C s^{-1}, refs. 11,15), owing to rapid thermal dissipation.

Most conventional solid-state synthesis techniques, including flux growth and chemical vapour deposition, involve the use of a resistive furnace[29]. Joule heating is used in heating elements embedded within the furnace, which act as the resistive medium through which current passes. These heating elements pass heat through the walls and gas inside the furnace through thermal conduction, convection and radiation, heating the chemical reactants within the furnace[29]. The slow heat-transfer rate limits the heating rate to a maximum of ~1 °C s^{-1}, and these furnaces have low thermal efficiency as the target reactants compose only a small minority of the total heat capacity of the volume being heated[29].

In contrast to furnace-based heating methods, FJH uses the materials themselves as the resistive medium, allowing for ~100% sample heating efficiency at heating rates up to 10^5 °C s^{-1} (ref. 11). This fast heating rate and the subsequent fast cooling rate enable kinetically controlled non-equilibrium products to be formed[15]. The high temperature of

FJH (in excess of 3,500 °C) allows for rapid reaction to be completed on a millisecond to second timescale[11,15]. Features including temperature range, heating and cooling rates, duration and heating manner distinguish FJH from conventional Joule heating (Box 1).

FJH is an electrothermal process rather than a solely thermal process. Therefore, in addition to temperature increase, FJH features the passage of electric current through the reactants, which necessitates an electrical potential difference through the sample rather than just

Box 1 | Resistance heating

Resistance heating, also known as resistive heating or Joule heating, has its roots in the 1840s when James P. Joule discovered that heat could be generated by applying electricity to a resistor[28]. Following Joule's law, heat (Q) produced is proportional to the square of the current (I) multiplied by the electrical resistance (R) of the resistor and the heating time (t),

$$Q = I^2Rt \quad (4)$$

Joule heating boasts a theoretical energy conversion efficiency (η) of 100%, meaning that all electric energy is converted into heat (see the table, which compares general resistive Joule heating with flash Joule heating (FJH)). This efficiency contrasts with the fuel utilization efficiency of furnaces, where chemical energy is transformed into heat through combustion. Furnace efficiency varies from 50% to 100% depending on the system design, but is often at the lower end of this range[179].

Resistive Joule heating is used in indirect heating resistance furnaces[29], which are widely used across industry, such as in metallurgy[29]. In these furnaces, current passing through a material generates heat, which is then transferred to the medium through conduction, convection and/or radiation[29]. Enclosures are typically used to isolate the heating process from the external environment[180]. However, indirect resistance heating tends to have low energy efficiencies due to heat loss during the transfer process.

Unlike indirect Joule heating, direct Joule heating[10] involves no intermediate heat transfer and therefore has very high energy efficiency. Direct heating for materials synthesis is used in the carbothermal shock process[105,106]. This process involves the loading of metal feedstocks on a carbon substrate, followed by introduction of an electric pulse for rapid heating, resulting in nanoparticle synthesis. The feedstocks are in direct contact with the carbon paper, and heated by mainly conduction. The carbothermal shock method has been widely applied in the production of nanomaterials[105,114,116,125], ceramic processing[38,181], thermochemical synthesis[130] and plastic depolymerization[149]. FJH is another type of direct Joule heating and uses high temperatures and a fast duration (see the table). In addition to the direct contact heating, FJH can use the materials themselves as the resistive medium. In this case, heat transfer is not required, such that the efficiency can be even higher than the carbothermal shock process. Many other terms are used in the literature, such as high-temperature shock, high-temperature sintering, high-temperature electrothermal process, flash carbothermic reduction, flash upcycling, flash sintering and rapid Joule heating; some of these processes can have indirect characteristics or variations of carbothermal shock and FJH.

Feature	Combustion furnace[a]	Resistance furnace	Carbothermal shock	Flash Joule heating
Energy source	Combustion of fuel	Continuous electric current	Short, high-power electric pulse	Short, high-power electric pulse
Electricity supply	Not required	d.c. or a.c. power	d.c. or a.c. power	d.c. or a.c. power, capacitor
Principle	Exothermic chemical reaction, heat transfer	Joule's law of heating, heat transfer	Joule's law of heating, heat transfer	Joule's law of heating, with or without heat transfer
Maximum energy efficiency	Moderate, up to 80–90% (ref. 182)	High, up to 95–100%	High, up to 95–100%	High, up to 95–100%
Temperature range	Depending on the fuel types, typically <2,000 °C (ref. 183)	Up to 3,000 °C	Up to 3,000 °C	Up to 3,500 °C
Heating rate	Slow, typically <50 °C min^{-1}	Slow, typically <30 °C min^{-1} for a resistance furnace[184]	Extremely high, up to 10^5 °C s^{-1}	Extremely high, 10^2–10^5 °C s^{-1}
Cooling rate	Slow, typically <10 °C min^{-1}	Slow, typically <10 °C min^{-1} for a resistance furnace	Extremely high, up to 10^4 °C s^{-1}	Extremely high, 10^2–10^4 °C s^{-1}
Processing duration	Long, typically hours	Long, typically minutes to hours or days	Short, typically milliseconds to minutes	Short, typically milliseconds to minutes
Heating manner	Indirect heating	Indirect heating, mainly by convection and radiation	Direct heating by thermal conduction heating	Direct heating by Joule resistance heating or thermal conduction heating
Material suitability	Wide applicability	Conductive and semiconductive materials	Materials loaded onto a carbon substrate	Materials with appropriate resistance (typically ~0.5–10 Ω, although larger ranges can be used depending on the power supply methods) or materials in direct contact with a resistance heat source

[a]Combustion furnaces do not use Joule heating and are discussed here as a comparison.

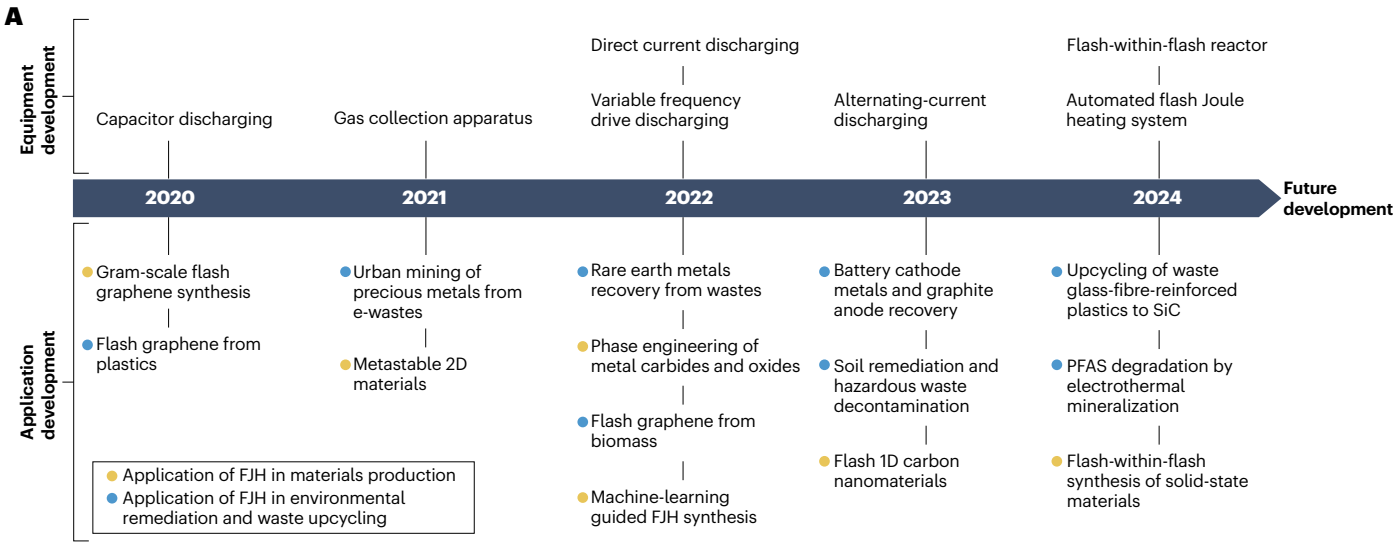
A
Equipment development
Capacitor discharging
Gas collection apparatus
Direct current discharging
Variable frequency drive discharging
Alternating-current discharging
Flash-within-flash reactor
Automated flash Joule heating system
2020
2021
2022
2023
2024
Future development
Application development
Gram-scale flash graphene synthesis
Flash graphene from plastics
Urban mining of precious metals from e-wastes
Metastable 2D materials
Rare earth metals recovery from wastes
Phase engineering of metal carbides and oxides
Flash graphene from biomass
Machine-learning guided FJH synthesis
Battery cathode metals and graphite anode recovery
Soil remediation and hazardous waste decontamination
Flash 1D carbon nanomaterials
Upcycling of waste glass-fibre-reinforced plastics to SiC
PFAS degradation by electrothermal mineralization
Flash-within-flash synthesis of solid-state materials
Application of FJH in materials production
Application of FJH in environmental remediation and waste upcycling

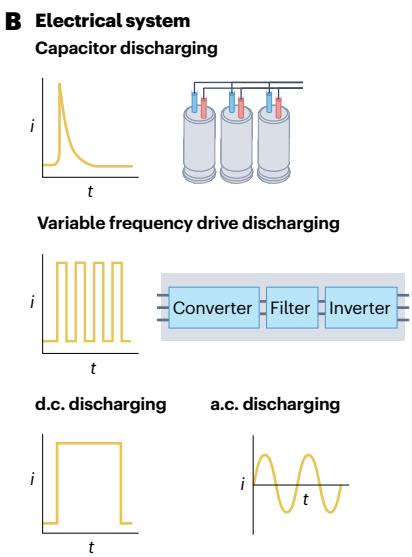
B Electrical system
Capacitor discharging
i
t
Variable frequency drive discharging
Converter
Filter
Inverter
d.c. discharging
a.c. discharging

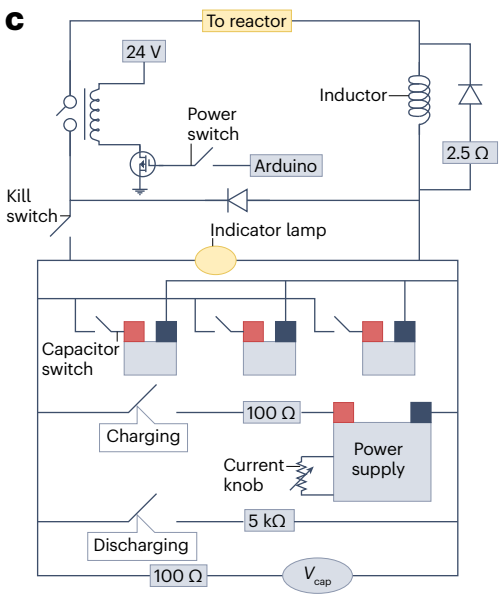
C
To reactor
24 V
Inductor
Power switch
Arduino
2.5 Ω
Kill switch
Indicator lamp
Capacitor switch
100 Ω
Charging
Power supply
Current knob
5 kΩ
Discharging
100 Ω
V_{cap}

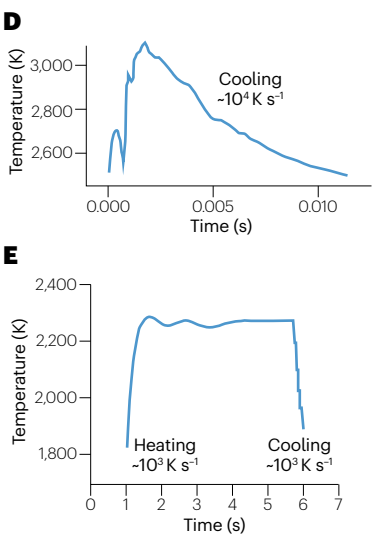
D
Temperature (K)
3,000
2,800
2,600
Cooling ~10⁴ K s⁻¹
0.000
0.005
0.010
Time (s)
E
Temperature (K)
2,400
2,200
2,000
1,800
Heating ~10³ K s⁻¹
Cooling ~10³ K s⁻¹
0
1
2
3
4
5
6
7
Time (s)

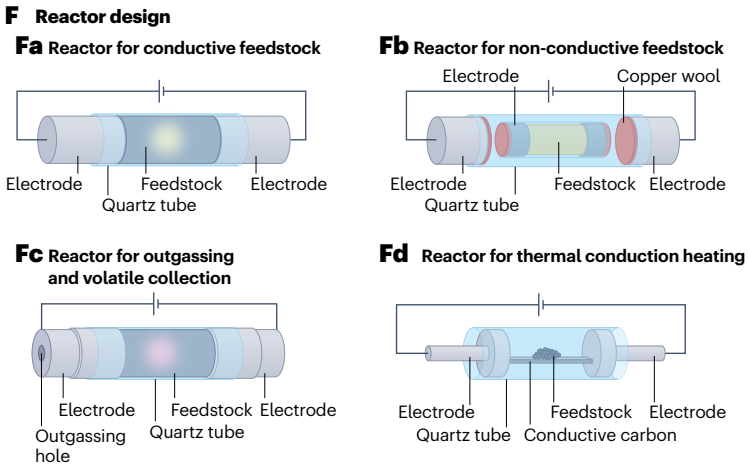
F Reactor design
Fa Reactor for conductive feedstock
Electrode
Feedstock
Electrode
Quartz tube
Fb Reactor for non-conductive feedstock
Electrode
Copper wool
Electrode
Feedstock
Electrode
Quartz tube
Fc Reactor for outgassing and volatile collection
Electrode
Feedstock
Electrode
Outgassing hole
Quartz tube
Fd Reactor for thermal conduction heating
Electrode
Feedstock
Electrode
Quartz tube
Conductive carbon

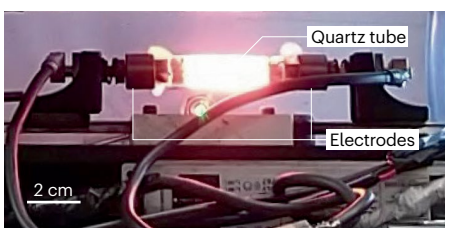
G
Quartz tube
Electrodes
2 cm

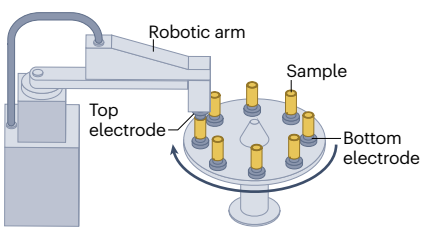
H
Robotic arm
Sample
Top electrode
Bottom electrode

Fig. 1 | FJH principle, equipment and scale-up. Various feedstocks, reactor set-ups and electrical systems can be used depending on the target reaction and product. **A**, Historical development of flash Joule heating (FJH), including equipment and application developments. **B**, Four types of electric systems for current input: capacitor discharging for a single-pulse discharge; variable frequency drive enabling discharging with pulse-width modulation; constant d.c. discharging; and a.c. discharging. Capacitor discharging provides a higher but time-limited power input compared with a.c. or d.c. discharging; variable frequency drive provides an ultrashort pulse input, down to milliseconds; d.c. discharging and a.c. discharging enable continuous heating, but the power is limited. **C**, Electronic diagram of a capacitor-based FJH system. **D**, Temperature profile of typical capacitor discharging. **E**, Temperature profile of typical d.c. discharging. **F**, FJH reactor designs. For conductive feedstocks or mixtures of non-conductive feedstocks with conductive additives, current directly passes through the materials for direct heating (panel **Fa**). For non-conductive feedstocks, heating elements are used to heat the sample, such as in the flash-within-flash reaction chamber (panel **Fb**) and carbon sheet design (panel **Fd**). For outgassing and volatile collection, an electrode with a through hole is used (panel **Fc**). **G**, Reactor and intense light emission during the FJH process. **H**, Automated loading and unloading system used to synthesize flash graphene for automated synthesis. *i*, current; PFAS, perfluoroalkyl and polyfluoroalkyl substances; SiC, silicon carbide; *t*, time; V_{cap}, voltage of the capacitor. Panels **C** and **D** adapted from ref. 11, Springer Nature Limited. Panel **E** adapted with permission from ref. 39, CC BY 4.0. Panel **Fb** reprinted from ref. 20, Springer Nature Limited. Panel **G** adapted with permission from ref. 23, Wiley.

along a sample surface. The presence of an electric current passing through a material affects the chemical products[13] and can lower reaction activation energies by as much as 50% (ref. 30). The passage of current through the material also promotes crystalline alignment of the flash-Joule-heated product along the axis of current flow, and this effect is further enhanced through rapid pulse-width modulation[31]. With the same current and voltage input, Joule heating performance depends on various materials properties, including thermal conductivity, a defined resistivity range and heat capacity, so the temperature is related to the materials.

Electric systems and hardware

FJH can be performed with any system that applies a sufficient voltage across the reactant medium. The methods were initially developed using capacitor-based systems[11] (Fig. 1B). The energy delivered is determined by the total capacitance of the capacitors as well as the voltage to which these capacitors are charged prior to discharging, as expressed in equation (1):

$$E = \frac{1}{2}CV^2 \quad (1)$$

where E is the energy input, C is the capacitance and V is the voltage.

The advantages of a capacitor-based system include the precisely controllable timescale of power delivery through associated electronics (Fig. 1C), the controllable predetermined energy value, and the ability of many models of capacitors to be charged to several hundred volts. Consequently, capacitor-based systems can achieve high power output, up to 1 MW (ref. 23), but are limited in output duration (usually subsecond timescales)[11]. Engineering techniques, such as pulse-width modulation by a variable frequency drive (Fig. 1B), can increase the capacitor discharge duration. Capacitor-based FJH systems can effectively be scaled up to kilogram production using rapid cycling of smaller batches, with automated sample loading and unloading to make the system continuous and high throughput. In these systems, the rate-determining step is often the repeated recharge time of the capacitor bank after each use[23,32].

Non-capacitor systems have the benefit of allowing continuous FJH without a necessary recharging step, offering higher energy delivery—despite reduced power output—owing to the long FJH timescales permitted (Fig. 1B). These non-capacitor, continuous systems exist in alternating-current (a.c.) and direct-current (d.c.) varieties (Fig. 1B). Alternating-current flash Joule heaters use a.c. electricity directly from the laboratory or manufacturing site, and they do not rectify the current before delivering it through the sample. Such systems are commonly used for pretreatment to reduce the electrical resistivity of a sample before subsequent d.c. flashing[33,34]. Direct-current systems feature a device that rectifies the a.c. input from the facility to d.c. output to the sample and are the most common type of continuous flash Joule heater[24]. These systems have programmable power supplies with which the desired voltage and current can be chosen before the reaction, and they can be programmed to adjust during FJH. In this way, continuous systems offer superior energy controllability and output relative to capacitor-based systems, while having inferior power output. Indeed, a capacitor-based FJH reaction can be completed in milliseconds (Fig. 1D), whereas an a.c.-based or d.c.-based FJH reaction can be sustained much longer (Fig. 1E).

Reactor design

Most FJH reactions involve filling the reactant feedstock into an FJH vessel, consisting of an insulative tube capped at the two ends by FJH electrodes made of either brass or graphite (Fig. 1Fa). Although other materials such as polytetrafluoroethylene are occasionally used[35], the tube is typically fused quartz in laboratory settings, as its transparency allows for convenient observation and temperature measurement of the reaction through infrared and spectral methods. Fused quartz also has a high melting point (~1,650 °C), but this is rarely reached as minimal heat is transferred to the tube during the rapid FJH reaction. Additionally, the low thermal conductivity and low thermal expansion coefficient of fused quartz allow it to withstand cracking from thermal shock caused by rapid heating and cooling of FJH reactions. For large-scale applications, other refractory, cost-effective materials such as concretes, ceramics or brick might be used.

Before FJH, the feedstock is compressed between the electrodes to improve electrical contact and reduce the sample resistance[11]. Vessels can either be sealed to contain the gaseous products of the flash reaction or instead have holes in the electrodes to allow pressure relief through reaction outgassing (Fig. 1Fc). Most FJH reaction vessels are deliberately not sealed to allow reaction outgassing and prevent high pressure buildup within the reaction vessel. This outgassing is often advantageous in removing volatile reactant impurities, resulting in higher product purity[26,33]. Furthermore, outgassing prevents oxygen infiltration, protecting the reactants and products from burning at the high temperatures reached. The volatiles can also be collected for analysis of the reaction process. In some cases, the volatiles are the desired products[36].

The electrical current exhibited during an FJH reaction is a function of the bulk resistance of the sample and the output voltage of the

FJH system, both of which determine the current value, as described by Ohm's law:

$$\frac{V}{R} = I \quad (2)$$

where I is the current, V is the voltage and R is the sample resistance. If the sample resistance is too high, the current value could be too low, and thus the power delivered will not be sufficient, as described by Joule's law:

$$P = \mathrm{IV} = I^2R \quad (3)$$

where P is the power. By contrast, if the sample resistance is too low, then a substantial portion of the heating can occur in the components of the FJH system rather than in the sample. Hence, the sample resistance should be in a suitable range for delivering the most electric energy. The real-time temperature profile during the FJH reaction is usually recorded using an infrared thermometer or a spectrometer when the temperature exceeds 3,000 °C (refs. 11,15).

As resistivity is an intrinsic property of a material, the requirement of sample resistance could restrict the applicable feedstock. To address this limitation, several techniques have been developed for non-conductive feedstocks. First, a low-power pretreatment heating step enhances the conductivity of carbon feedstocks through carbonization, which is especially useful when plastic or biomass are used as the feedstocks[37]. Second, the addition of conductive additives, typically carbon materials, into the feedstocks[33] permits the synchronous heating of the non-conductive material. In addition to carbon, other materials with appropriate resistance may be used as the substrates or additives for FJH, but this is underexplored in the field. The conductive additive can remain in the product in some cases, or it can be separated based on the property differences between the additive and the product, such as through sieving if their sizes are different. Third, the use of a resistive heating element enables the rapid heating of the non-conductive materials in thermal contact with it (Fig. 1Fb) or on it enabled by thermal conduction[20,30,38] (Fig. 1Fd). A preferred sample resistance for capacitor-based FJH systems is 0.5 to 10 Ω (ref. 11); when an a.c.-based or d.c.-based FJH system is used, a wide resistance range (0.05–100 Ω) can work, depending on the power supply[12].

Scale-up and industrial implementation

FJH is theoretically scalable[15,22,39]. Experimentally, FJH has been conducted at various scales. In its early demonstration for flash graphene synthesis[11], which used a capacitor-based system with a total capacitance of 0.06 F and a maximum voltage of 200 V, the mass of product ranged from 0.03 g to 1 g per batch. For a capacitor-based system, the voltage and/or capacitance of the capacitors can be increased to increase the mass per batch: 10 g per batch of flash graphene was prepared using an upgraded FJH system with a capacitance of 0.624 F and a maximum voltage of 480 V (ref. 23) (Fig. 1G). Furthermore, a lab-scale automated FJH system[23] has been demonstrated to achieve the synthesis of flash graphene using metallurgical coke as the feedstock at a production rate of 730 g h^{-1} (ref. 23). Continuous FJH models have been introduced for flash graphene synthesis[40], including a continuous automatic device for flash graphene synthesis from biomass with a production rate of 21.6 g h^{-1} (ref. 37) (Fig. 1H).

Integrating continuous d.c. or a.c. into the FJH process offers better energy deliverability than a capacitor-based FJH system and enables scale-up, provided there is a sufficient instant power supply. For example, mass scales of 100 g per batch have been achieved using an a.c. FJH heater[25]; a US$530 continuous FJH reactor was used to achieve 5 kg h^{-1} flash graphene synthesis from metallurgical coke at kilogram-scale batch size[41]. Although lab-scale equipment is usually designed for manual operation, mechanical operation was integrated for continuous feedstock loading, FJH and product unloading for reported scale-up prototypes (Fig. 1h). Commercial scaling-up of the FJH process for flash graphene synthesis and metal recycling is ongoing. Broadly, we expect further scale-up of the FJH process for graphene production as well as other uses in the near future, given the automation equipment development, engineering advances and investment in this field.

Owing to the high-power input and high intensity of the reaction during the FJH process, there is a risk of electric shock, explosion, burns or eye damage if the electricity supply system and reactor are not properly designed, managed and used with appropriate precautions (Supplementary Note 1). Safety is paramount to the equipment design and operation, and while a 10-g scale per batch has been realized on the laboratory scale, further scaling requires due precautions. In particular, FJH users should gradually increase the energy input rather than begin reactions at maximum input, especially for these reactions with intense outgassing[23].

Production of graphene and related carbon materials

FJH was originally developed for graphene production and is widely used in flash graphene synthesis[11,14,37]. Related carbon materials are also synthesized via FJH, as the ultrahigh temperature makes it especially useful for carbon materials production: almost all carbon resources, including carbon black[11], hard carbon[42], coal[43,44], coke[23], plastic[33], rubber[45], biomass[46], food[11], CO_2-derived amorphous carbon[47], pyrogenic carbon[48], and municipal solid waste[49], are graphitized below 3,000 °C. Moreover, the temperatures reached during FJH can cure material defects and volatilize out impurities, so that the quality of the carbon material produced is usually good to excellent[50]. By tuning the feedstock and optimizing FJH parameters, several carbon morphologies, including graphene, graphite, carbon nanotubes, carbon nanofibres, and their doped or mixed counterparts, have been synthesized (Fig. 2a and Supplementary Table 2).

Flash graphene production and characterization

Flash graphene is made when an amorphous carbon feedstock, commonly from low-value or waste feedstocks such as coal, coke, plastics or biomass, is heated to 2,000–3,000 °C to induce conversion into turbostratic flash graphene (Fig. 2b)[11]. In contrast to ordered graphene[51,52], turbostratic graphene layers are randomly angularly displaced with respect to each other, resulting in increased interlayer spacing and lowering the van der Waals interactions between the layers. This disordered stacking arises from the kinetic trapping of the graphene layers due to the rapid heating and cooling rates[11,30].

Turbostratic graphene can have an arbitrary number of layers that remain optically and electronically decoupled. Hence, it has electronic properties more similar to those of monolayer graphene than multilayer graphene, owing to that interlayer decoupling[11,53–56]. For example, both monolayer and turbostratic graphene are zero-bandgap semiconductors and can support massless Dirac fermions, in contrast to multilayer graphene. These similarities in electronic properties result in similar Raman spectra of monolayer and turbostratic graphene

a

Carbon feedstock	Additives/catalysts	FJH process	Carbon materials product
Conductive carbon (such as carbon black, coal and coke)	None	Capacitor FJH, 50 ms to 1 s typically 2,500–3,000 °C	Turbostratic flash graphene
Non-conductive carbon (such as plastic, rubber, biomass and food)	Carbon conductive additives	Step i: a.c. FJH for outgassing Step ii: Capacitor FJH	Turbostratic flash graphene
Plastic	Carbon conductive additives, $Ca(OAc)_2$ etchant	Step i: a.c. FJH for outgassing Step ii: Capacitor FJH	High-surface-area flash graphene
Conductive carbon (such as carbon black)	Dopant (such as melamine, phosphorus and boron)	Capacitor FJH	Heteroatom-doped flash graphene
Plastic	Carbon conductive additives, catalysts (such as Fe and Ni)	Capacitor FJH	Carbon nanotubes and nanofibres

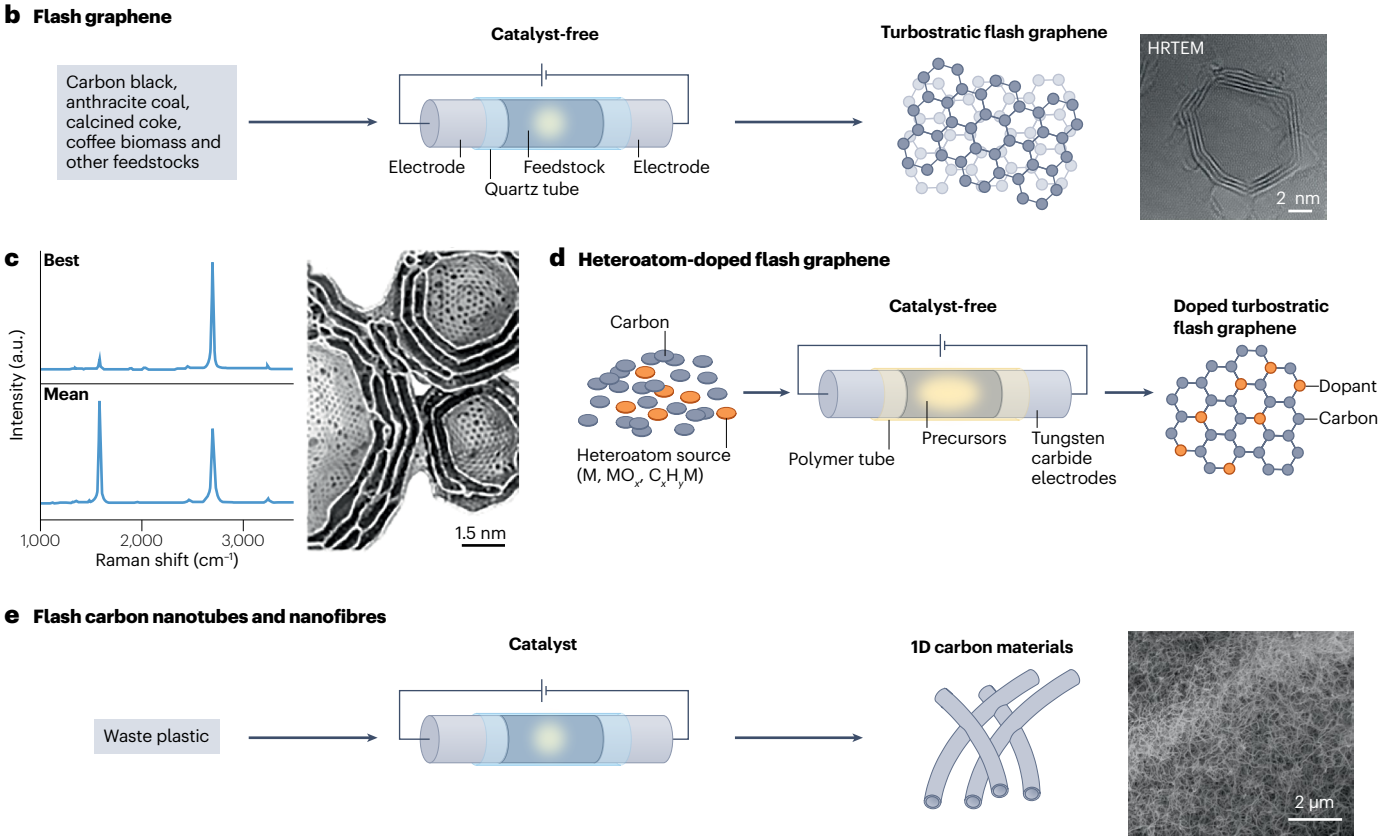

Fig. 2 | FJH for graphene and related carbon materials synthesis. Flash Joule heating (FJH) was initially demonstrated in flash graphene synthesis and has subsequently been applied in the synthesis of other carbon materials. **a**, Different carbon material products derived from different input of carbon feedstocks, additives or catalysts, and FJH conditions (complete list in Supplementary Table 2). **b**, The FJH process (left) and high-resolution transmission electron microscope (HRTEM) image (right) of flash graphene derived from carbon black. **c**, Characterization of flash graphene. Left, Raman spectra of calcined coke-derived flash graphene; right, simulated atomic structure of flash graphene. **d**, Synthesis of heteroatom-doped flash graphene. **e**, Flash carbon nanotube synthesis (left) with scanning electron microscopy image of carbon nanotube products (right). Panel **b** reproduced from and panel **c** adapted from ref. 11, Springer Nature Limited. Panel **e** adapted with permission from ref. 14, Wiley.

(Fig. 2c), which are distinct from the spectra of multilayer graphene or graphite[11] (Supplementary Table 3).

Flash graphene is characterized chiefly by Raman spectroscopy (Fig. 2c), which provides information on the crystallinity, defect density and turbostratic character. Specifically, the *D*, *G*, 2*D* (also known as *G′*)[57] and sometimes TS_1, TS_2 (turbostratic indicators) and M (AB-ordered stacking indicator) bands are examined. The 2*D* peak height is correlated with graphene crystallinity, and the $I_{2D/G}$ peak ratio is examined as one metric to determine conversion from amorphous carbon to graphene. Conventionally, an $I_{2D/G}$ of at least 0.3 is necessary for graphene conversion[58]. Turbostratic flash graphene typically exhibits a 2*D* band full-width half-maximum (FWHM) of ~15–30 cm^{-1} and a single Lorentzian peak shape[11], comparable to that of single-layer graphene (~24 cm^{-1}, ref. 57). Multilayer graphene exhibits an asymmetric 2*D* band composed of multiple Lorentzian peaks, and the 2*D* band FWHM of stacked graphene increases with the stacking number

such that four-layer graphene has a FWHM of ~40 cm^{-1} (ref. 57) and stacks even above 10 have a FWHM of up to 100 cm^{-1} (ref. 56). The best flash graphene samples show an undetectable *D* band and a high $I_{2D/G}$, demonstrating its low defect and high crystallinity (Fig. 2c, left). The TS_1 and TS_2 peaks are low-intensity and observed at ~1,880 cm^{-1} and ~2,030 cm^{-1}, respectively. The low-intensity M peak occurs at 1,760 cm^{-1}. When the two TS peaks and the M peak are simultaneously present in a sample, turbostratic and ordered stacking are present[30]. Carbon-13-enriched flash graphene shows an expected redshift in all of its Raman peaks due to the increased mass of the atoms, thereby decreasing their vibrational frequencies relative to those of conventional ^{12}C-flash graphene[59].

The structure of flash graphene can also be characterized using X-ray diffraction analysis[11] and transmission electron microscopy (TEM, Fig. 2b). Conventional ordered graphene, as obtained by graphite exfoliation, is a mixture composed of mostly Bernal (AB-stacked) graphene with a minority of rhombohedral (ABC-stacked) layers[60]. Each type has (100) and (101) X-ray diffraction peaks between ~41° and 46°; thus, most graphene samples show four small peaks in this region. In turbostratic graphene, the peaks associated with this region exhibit broadening compared to those of ordered graphene and thus overlap with each other[30]. In addition, layers of turbostratic flash graphene exhibit mixed moiré patterns under TEM, giving additional confirmation of the turbostratic stacking[11,61] (Fig. 2b).

The physical and spectroscopic characteristics of flash graphene vary with reaction parameters used in the FJH process, including power, energy[61] and the feedstocks (Supplementary Table 4). Graphene produced from low-energy input has a high interlayer spacing of ~0.341–0.343 nm, low crystallinity and high defect density, and exhibits wrinkles under TEM[61]. This rich morphology feature is distinct from graphene produced by chemical vapour deposition, which is often pristine[62] and ultraflat[63,64]. Graphene produced from moderate-energy FJH input has high crystallinity, a more sheetlike structure and lower defect density. With higher reaction energy, through either more intense flashes or longer duration, the turbostratic graphene is converted to ordered graphene (Bernal and rhombohedral) and graphite, with a lower defect density and interlayer spacing of 0.334 to 0.337 nm (refs. 30,65).

Flash graphene has been demonstrated in various applications, especially those that require bulk amounts of graphene. For example, flash graphene is used as an additive in cement composites that increases compressive strength by ~25% with just 0.05 wt% flash graphene addition[11]. It is also used in epoxy composites[66], concrete aggregate substitutes[67], lubricant additives[68], lithium-ion batteries[69] and conductive inks[70]. In addition to the preparation of pristine graphene, FJH is also adopted for an in situ graphene coating on other materials to enhance their performances. For example, graphene-coated Cu particles show enhanced oxidation resistance[71], and graphene-coated lithium iron phosphate has improved rate performance in batteries[72].

Modified and functionalized flash graphene

FJH carbon feedstocks can produce modified graphene products and different carbon nanostructures. For instance, heteroatom-doped flash graphene (an effective material in battery electrodes and supercapacitors[73]) is produced when a carbon feedstock is heated in the presence of a heteroatom-containing compound[21] (Fig. 2d). The doped graphene exhibits increased defect densities and an increased interlayer spacing relative to non-doped graphene[21]. Heteroatom doping ratios have been achieved above 10 at% (ref. 21).

When the feedstock is composed of a high proportion of non-carbon elements, such as boron or nitrogen, 2D turbostratic boron–carbon–nitrogen ternary compounds can be synthesized[74]. When a sealed flashing vessel is used, and the carbon feedstock is mixed with a fluorinated polymer, new carbon morphologies can be formed, including fluorinated nanodiamond, fluorinated graphene and fluorinated concentric carbon[35]. These different structures have a time evolution in which the nanodiamonds form first at ~10 ms, and concentric carbon forms last at ~1 s. Using solid-state relays with millisecond-scale controllability, the reaction can be stopped in 1-ms increments along any point of the evolution. The heteroatom functionalization strategies of FJH can be extended to other materials such as 2D transition-metal carbides[75], underscoring the versatility of FJH.

High-surface-area graphene is desirable for applications including electrocatalysis, battery anodes and sorption media. The flash graphene usually has a lower surface area than the feedstock, owing to thermal-induced aggregation of pores[76]. Typically, feedstocks with high surface area, such as carbon black, form higher-surface-area flash graphene[11] than do low-surface-area feedstocks such as coke[23]. Porous carbon and flash graphene synthesized from bituminous coal exhibit effective adsorptive properties[77,78].

High-surface-area flash graphene can be produced from engineered high-surface-area precursors. For example, FJH of graphene oxide can produce highly defective and, thus, high-surface-area graphene[79], and ultrafine metal nanoparticles can be decorated on a reduced graphene oxide aerogel when metal precursors are preloaded on it[80]. Similarly, when hollow mesoporous carbon spheres are used as feedstock, high-surface-area graphene hollow spheres can be produced with a surface area of up to 670 $m^2 g^{-1}$ (ref. 81). Another strategy uses an etchant during FJH to increase the surface area. In the presence of $Ca(OAc)_2$, FJH of plastics yields holey and wrinkled flash graphene with a surface area of up to 874 $m^2 g^{-1}$ and pore volume up to 0.32 $cm^3 g^{-1}$ (ref. 76). In another case, KCl/K_2CO_3 salts have been used for the molten-salt synthesis of porous carbon from anthracite by FJH, achieving a surface area of 1,338 $m^2 g^{-1}$ and pore volume up to 9.95 $cm^3 g^{-1}$ (ref. 82). As a comparison, activated carbon typically possesses a surface area of ~500–1,500 $m^2 g^{-1}$ and a pore volume of 0.3–0.8 $cm^3 g^{-1}$ (ref. 83).

One-dimensional carbon nanostructure synthesis

One-dimensional carbon materials, including multiwalled carbon nanotubes (CNTs) and bamboo-like carbon fibres, are formed when a carbon feedstock is treated by FJH in the presence of a CNT growth catalyst, such as iron or nickel[14] (Fig. 2e). The product formed from these reactions can be tuned by the FJH reaction temperature. A temperature of ~1,000 °C produces CNT without graphene; increasing temperature to ~2,000 °C leads to the formation of graphene–CNT hybrid structures; at temperatures beyond this, the ratio of CNT to flash graphene decreases such that virtually no CNTs remain by ~3,000 °C (ref. 14). Yield of CNT or hybrid morphologies, rather than 2D graphene morphologies, is estimated to be up to 90%, as observed by SEM imaging. Elemental purity of carbon can reach 98% even when waste plastics are used as feedstock[14]. Commercial multiwalled CNTs could range from 90% to 99% in carbon purity[84,85].

Further, FJH treatment can convert some of the CNTs into graphene. The conversion proportion is affected by the reaction duration and temperature. These CNT–graphene composites are effective reinforcing additives in epoxy composites[86]. Similarly, in the presence of a heteroatom-containing compound, heteroatom-doped CNT has been synthesized by FJH[32,87]. When ammonia borane is used as the feedstock,

boron nitride nanotubes can be produced[88]. Other carbon forms with different graphitization degrees and morphologies can be produced by FJH, such as hard carbon[89,90] and graphitic carbon cages[91].

Inorganic materials production

FJH is a versatile tool for phase engineering[15,35,92] as it has a broadly tunable energy input capable of reaching temperatures >3,000 °C. FJH-synthesized materials with rationally engineered morphologies and electronic structures have unique properties that position them, for example, as promising high-performance catalysts in renewable energy devices. This section discusses the synthesis of inorganic materials, including metastable materials, solid-state materials and nanocatalysts.

Synthesis of metastable materials

Metastable materials can be produced through rapid heating or cooling during FJH, as the system does not have enough time to reach equilibrium[93]. For instance, turbostratic flash graphene is a metastable phase as opposed to the more stable Bernal-stacked structures[94]. FJH is emerging as a tool for engineering other metastability, as well, such as structural dislocation and defects[95,96].

The temperature tunability of FJH allows access to many metastable phases by making them thermodynamically preferable. A notable example is the phase conversion of transition-metal dichalcogenides[92], where bulk conversion of molybdenum dichalcogenides (MoS_2) and tungsten dichalcogenides (WS_2) from 2H phases to 1T phases was achieved in milliseconds, reaching a phase ratio of up to 76%. The 1T phases are metastable with higher free energy than the 2H phases. FJH induces structural changes in the 2H phase, particularly the formation of sulfide vacancies, which reverses the thermodynamic preference[92]. A similar approach is used for the phase-controlled synthesis of transition-metal carbide nanocrystals[15]. The ultrahigh-temperature capability of FJH enables the carbothermic reduction of metal oxides, leading to the synthesis of metal carbides within 1 s (Fig. 3a, left). By controlling pulse voltages, phase-pure molybdenum carbides, including stable β-Mo_2C and metastable α-MoC1−x and η-MoC_{1-x}, can be selectively synthesized (Fig. 3a, right). Carbon vacancies introduced during the FJH process are the structural factor for the phase transition of carbides[15].

Beyond vacancies, FJH can precisely tune the morphology and size of inorganic nanomaterials, providing another route for phase engineering, such as in the phase transformation synthesis of high-surface-area corundum nanoparticles (Fig. 3b, left)[39]. Aluminium oxide (Al_2O_3) has an unusual surface-area-dependent formation energy: α-Al_2O_3 is the thermodynamically stable phase of coarse crystals, whereas γ-Al_2O_3 has a lower surface area, causing nanocrystalline Al_2O_3 to usually crystallize in the γ-phase[97]. The pulsed direct current input in the FJH process creates resistive hotspots at the interfaces between γ-Al_2O_3 nanoparticles (Fig. 3b, left), leading to controlled coarsening and an accompanying phase conversion from γ-phase to δ′-phase and then to α-phase (Fig. 3b, right).

The ultrafast cooling rate of the FJH process can kinetically retain the metastable phase at room temperature. This process is demonstrated by the kinetically controlled synthesis of metallic glass nanoparticles[18], as metallic glass can be obtained by rapid quenching[98]. Metal precursors loaded on a carbon substrate are subjected to FJH, rapidly raising the temperature; the resulting alloy melts and cools at an ultrafast rate (10^4 °C s^{-1}), vitrifying into glassy nanoparticles. Palladium-based and platinum-based metallic glass nanoparticles have been produced with this technique[18].

Rapid sintering and solid-state synthesis

Solid-state synthesis, also known as the ceramic method, is a reliable and versatile method for materials production[99] and typically yields thermodynamically stable phases[99]. FJH is useful in solid-state synthesis owing to its ultrahigh-temperature capability and rapid heating rates, which secure the thermodynamic spontaneity of many reactions and enable fast diffusion and reaction kinetics. However, most feedstocks are not conductive enough for FJH, necessitating unique designs to deliver electricity and heat to the feedstock.

Graphite sheets are used as the heating element for ceramic sintering (Fig. 3c, top). Resistance heating is already widely used in flash sintering[100] and spark plasma sintering[101]. Joule-heating-based sintering techniques can be faster, achieve higher temperatures and require less expensive apparatus[38]. In a typical high-temperature sintering set-up, the pressed pellet of a ceramic precursor powder is sandwiched between two woven graphite sheets, which rapidly heat the pellet by conduction and radiation (Fig. 3c, bottom)[38]. The sintering can be completed in seconds, making it especially promising for solid-state electrolytes to prevent loss of volatile elements such as lithium[38,102]. Rapid Joule-heating-based sintering has also been used to construct interfaces between solid electrolytes and cathodes, overcoming large interfacial resistances[103]. In addition, Joule-heating-based sintering has been previously explored in structural ceramic sintering, such as alumina ceramics from corundum nanoparticles[39]; however, the densification is relatively poor because of the limited sintering time. Joule-heating-based sintering would be useful for sintering ceramics that have volatile element components but less stringent requirements for densification.

Flash-within-flash (FWF) Joule heating has also been developed for inorganic synthesis[20,104] (Fig. 3d). The FWF process involves two quartz vessels: an outer vessel filled with conductive additives and an inner vessel loaded with feedstocks for the solid-state synthesis (Fig. 3d, left). The current applied to the outer vessel generates intense heat, which is then transferred through an inner vessel to the inner feedstock by conduction and radiation to drive chemical reactions. Thus, FWF is an indirect heating method. The FWF can be used multiple times or in an anion-exchange mode (Fig. 3d, right). FWF is a versatile, efficient and scalable method for the production of phase-selective, single-crystal bulk powder materials at the gram scale, as demonstrated by the synthesis of ten transition-metal dichalcogenides, three group XIV dichalcogenides and nine non-transition-metal dichalcogenide materials[20]. In the FWF configuration, metal precursors are not in contact with the carbon in the outer tube, so metal carbide formation is mitigated. These two designs — woven graphite sheet heating elements and outer–inner tube FWF configurations — enable the use of non-conductive materials, or even materials that are too conductive, greatly expanding the versatility of the FJH process. These methods rely primarily on thermal conductive heating, but rapid heating rates and efficiencies differentiate them from traditional furnace heating methods.

Carbon-supported inorganic nanocatalysts

Inorganic nanomaterials can be synthesized by FJH, typically using carbon materials such as carbon black[18] and carbon nanofibre[105] as conductive additives and substrates, as their electrical resistance makes them suitable for Joule heating. After loading precursors onto the carbon support, the current passing through the carbon instantly generates heat. The heat leads to the decomposition, reaction and fusion of the precursors, and then solidification to form nanoparticles during the cooling stage[105]. Various inorganic nanomaterials have been produced using

a **Phase-controlled synthesis of transition metal carbide nanocrystals**

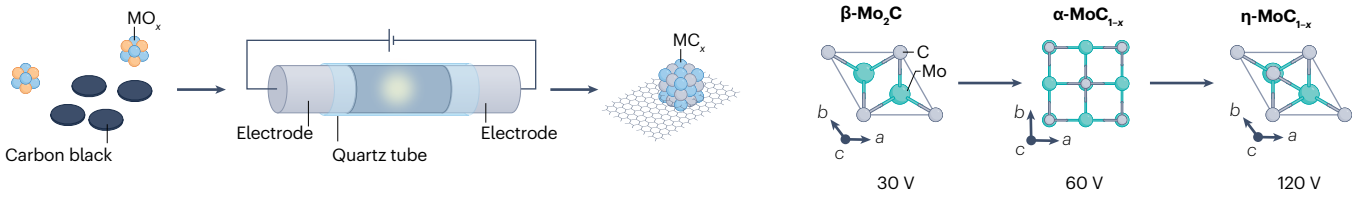

b **Phase engineering of alumina for high-surface-area corundum nanoparticles**

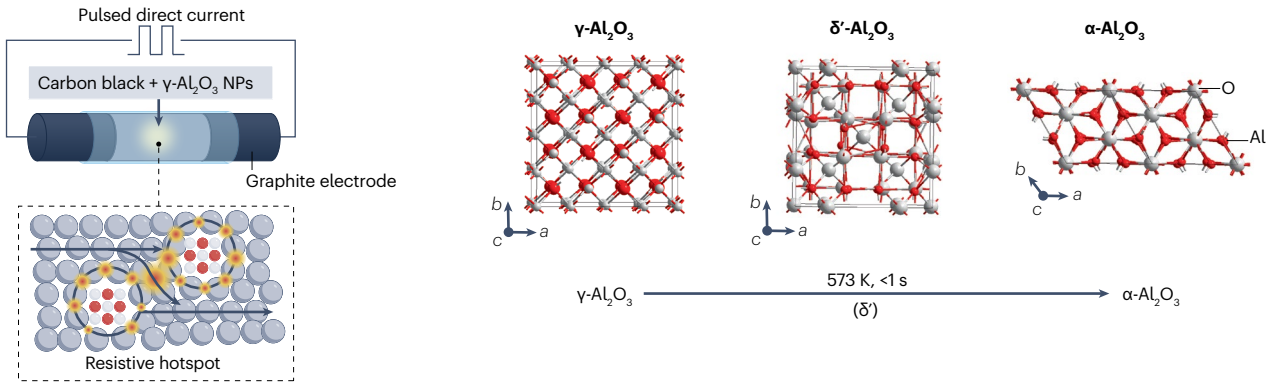

c **Rapid Joule heating sintering process for ceramic synthesis**

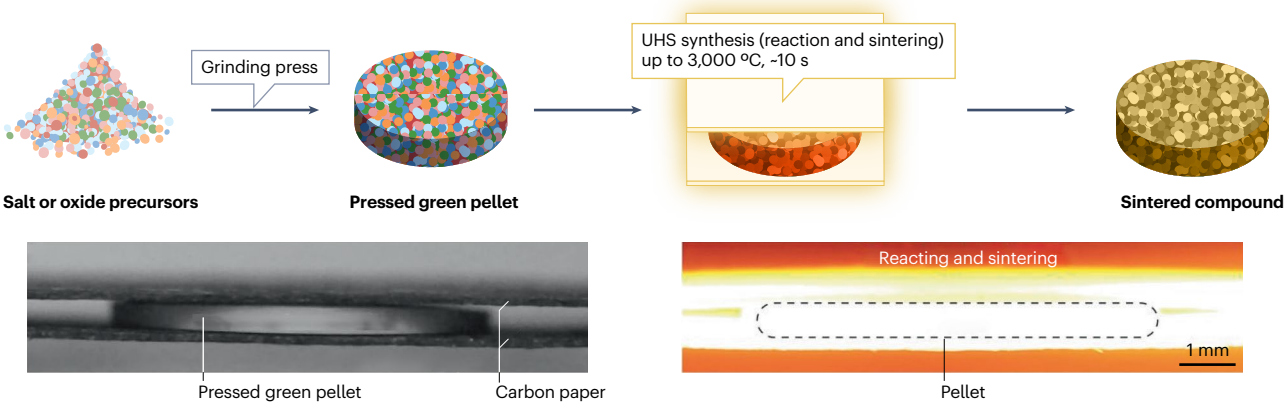

d **Flash-within-flash Joule heating for bulk synthesis of transition-metal dichalcogenides**

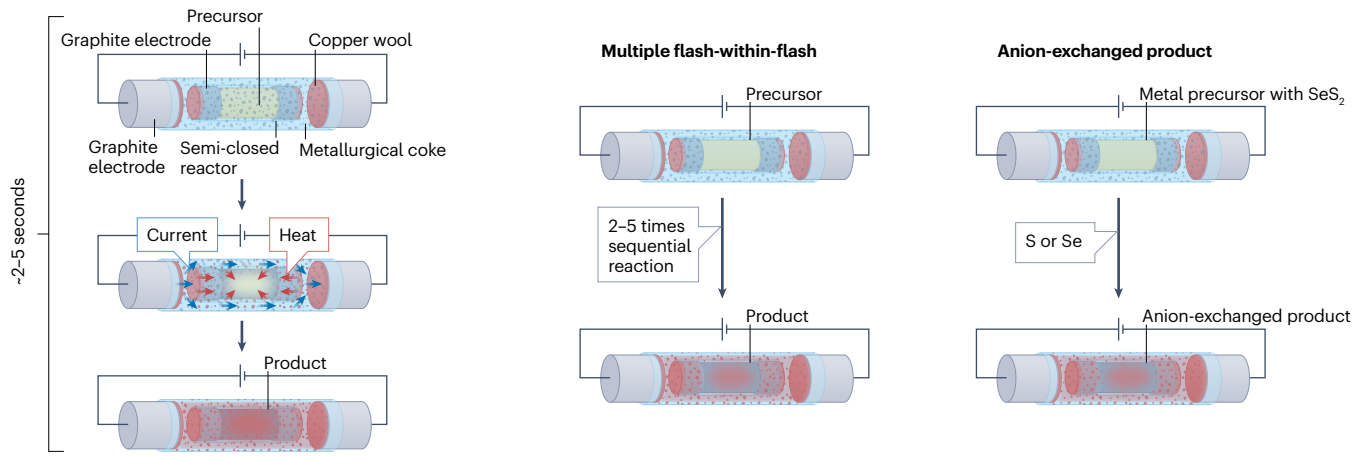

Fig. 3 | FJH for phase-controlled synthesis of functional inorganic materials. Inorganic materials can be synthesized using various flash Joule heating (FJH) techniques. **a**, FJH synthesis of metal carbides using metal oxides and carbon black as feedstocks (left), and the phase transformation from β-Mo_2C to α-MoC_{1-x} to η-MoC_{1-x} with the increase of FJH voltage (V) input (right). **b**, Pulsed direct-current heating and resistive hotspot at the gap of mixture of γ-Al_2O_3 and carbon black (left) and the phase transformation from γ-Al_2O_3 to δ′-Al_2O_3 to α-Al_2O_3 (right). **c**, Ultrahigh-temperature sintering (UHS) process, in which the pressed green pellet is placed between two sheets of carbon paper and heated to 3,000 °C for 10 s. Photographs show the set-up at room temperature and at ~1,500 °C. **d**, Flash-within-flash (FWF) Joule heating system is composed of an outer tube for Joule heating of carbon and an inner tube for the desired reaction (left). Other FWF processes include the multiple FWF reaction (middle) and anion-exchange FWF reactions (right). NP, nanoparticle. Panel **a** reprinted from ref. 15, CC BY 4.0. Panel **b** adapted from ref. 39, CC BY 4.0. Panel **c** adapted with permission from ref. 38, AAAS. Panel **d** adapted from ref. 20, Springer Nature Limited.

this method, including single metals[96,106–109], multimetallic alloys[110,111], metallic heterostructures[112,113], high-entropy alloys[105,114,115], single atoms[116], and metallic compounds[117] such as sulfides[118], oxides[119,120], selenides[121] and carbides[117,118,122].

The precise control of reaction time down to milliseconds during FH allows for the formation of dispersed, ultra-small particles by preventing their agglomeration[105]. The carbon supports are vital for the dispersion and stability of nanoparticles by providing numerous nucleation and binding sites[123,124]. Moreover, as FJH is a dry process, the surface of the as-produced nanomaterials remains clean, in contrast to materials synthesized by wet chemistry, which are often contaminated by surfactants and capping agents[18]. Their cleanliness and structure make the FJH-produced materials suitable for use as catalysts in a variety of applications, including thermal catalysis[114,115], electrocatalysis[95,107,111,118,125], environmental catalysis[108] and photocatalysis[126,127].

FJH is primarily used for solid-state synthesis, but with proper reactor design it can be integrated into wet chemistry and gas reactions. A wet-interfacial Joule heating approach has been proposed to synthesize various nanomaterials from solution feedstocks[128,129]. By instantaneous evaporation of solvents that are on the carbon heater, synthesis is completed in <1 s (ref. 128). For thermochemical synthesis, a non-equilibrium synthesis that uses programmable electric current to rapidly heat and quench gas reactions has been demonstrated[130], achieving methane pyrolysis with high selectivity to C_2 products.

Resource recovery and waste upcycling

Thermal treatment is commonly used in resource recovery and waste upcycling[131]. However, increased energy efficiency and reduced costs and emissions are needed to ensure that the value of the recovered products can offset the process costs. FJH is therefore being explored for the recovery of metals from waste streams such as electronic waste (e-waste), industrial wastes and spent batteries[22,27,36,132,133], the upcycling of inorganic wastes[22,134], and the conversion of carbonaceous waste (such as plastics and rubbers) into graphitic materials[12,33].

Metal recovery and inorganic waste upcycling

Metals are often the most valuable and recoverable components of waste[135]. Their recovery involves altering their chemical forms, speciation, and distribution to enable their separation from wastes based on property differences. FJH, with its high-temperature capability and cost-effectiveness, makes these conversions feasible and economic[36].

Critical metals recovery from e-waste and industrial wastes. FJH in metal recovery was originally demonstrated in urban mining, through the gram-scale recycling of precious metals from e-wastes — specifically, waste printed circuit boards[36]. The difference between the vapour pressures of metals and those of the substrate materials (carbon, ceramics and glass) allows the separation of metals, which is called evaporative separation. Precious metals in e-wastes are heated and evaporated by ultrahigh-temperature FJH; then the metal vapours are transported and condensed in a cold trap (Fig. 4a). With the assistance of chlorination (converting the metal into its chloride by reacting with chlorinating agents), recovery yields of >80% were achieved for rhodium, palladium, silver and gold within 1 second (ref. 36).

Integration of FJH into an electrothermal chlorination or electrothermal carbochlorination process is performed for selective separation of critical metals from waste feedstocks[136]. The electrothermal chlorination process leverages the differences in the free energy of formation of metal chlorides as well as the kinetic selectivity due to the ultrafast heating and cooling capability of FJH. This process has been demonstrated in the recovery of gallium, indium and tantalum from e-wastes with purities >95% and yields >88% (ref. 136).

FJH has also been used to recover rare earth metals from coal fly ash[27], a by-product of coal combustion. In this process, FJH thermally converts the hard-to-dissolve rare earth phosphates into rare earth oxides and metals with high solubility (Fig. 4b). The FJH activation increased the recovery yield of rare earth metals roughly twofold compared with directly acid leaching the raw materials. This method is also applicable to other wastes like e-wastes and bauxite residues (red mud)[27].

Recycling and regeneration of spent batteries. Battery cathodes can be recycled through hydrometallurgy, which typically involves acid leaching of metals. However, the transition metals in active cathode materials with high valence states lead to low leaching efficiency[137]. FJH has been applied to make this process more efficient by heating the black mass, which is the combined anode and cathode waste routinely used in the recycling industry[132] (Fig. 4c). This process led to the thermal decomposition of the compact solid–electrolyte interphase (SEI) and the carbothermic reduction of the spent cathode materials ($LiNi_xMn_yCo_{1-x-y}O_2$, $LiCoO_2$, $LiNi_xCo_yAl_{1-x-y}O_2$ and $LiFePO_4$) into their lower oxidation state or metallic form. With this FJH activation, the metal recovery yield was improved from <35% to >98% (Fig. 4c).

Direct recycling (regeneration of battery materials without destroying their crystal structures) has gained attention due to potential reduced environmental impacts and economic costs relative to destructive recycling such as hydrometallurgy[138]. High-temperature calcination that gasifies organics for graphite anode regeneration is technically straightforward[139], but as graphite is less valuable than cathode materials, furnace-based extended calcination is often not economically viable[139]. FJH has been applied to decompose the impurities and regenerate the entire graphite anode in 1 second, which significantly reduces the energy consumption and carbon emission compared with high-temperature calcination recycling[140] (Fig. 4d). The recycled anode preserves the graphite structure while being coated with an SEI-derived carbon shell, contributing to high battery performance[133].

Another FJH-based process involves converting the loose SEI layer that is coated onto the degraded graphite into a compact and mostly inorganic mass that encloses active lithium, leading to >100% initial

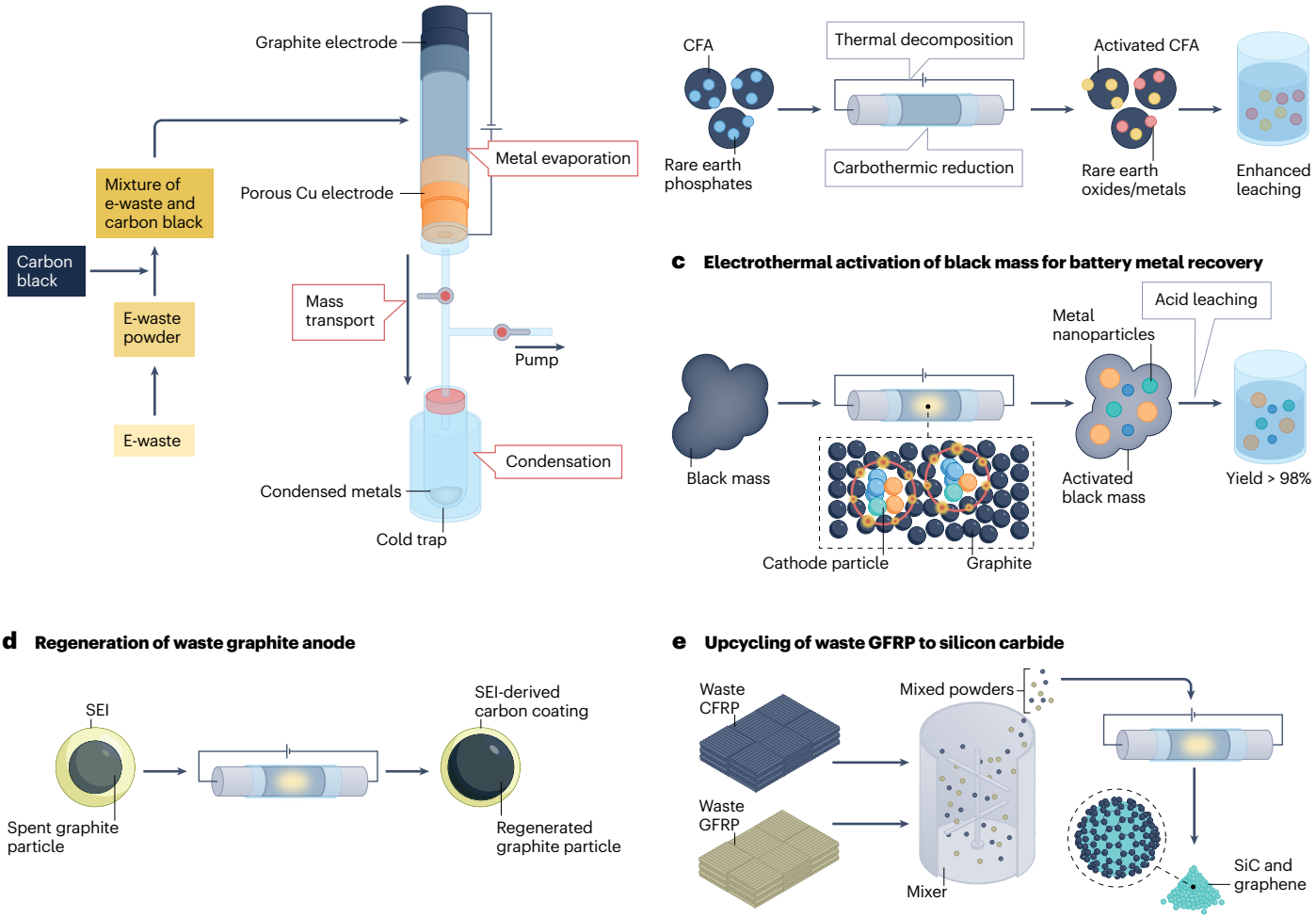

Fig. 4 | Metal recovery and waste upcycling by FJH. Critical metals and batteries can be recovered from waste streams, and solid waste can be repurposed to value-added products by flash Joule heating (FJH). **a**, The FJH urban mining and metal evaporative separation system. The system is composed of three parts, including FJH for metal evaporation, the vacuum system for mass transport and the cold trap for condensation of volatiles. Electronic waste is ground into fine powders and then mixed with carbon black. **b**, Electrothermal activation of coal fly ash (CFA). Rare earth phosphates in the CFA raw materials are converted to rare earth oxides or metals by thermal decomposition and carbothermic reduction, leading to a rare earth recovery yield twice as high as for directly acid leaching the raw materials. **c**, FJH activation of black mass composed of graphite and cathode particles (left), and the extraction of metals by acid leaching of the FJH-activated materials (right). The activation increases the yield from <35% to >98%. **d**, Regeneration of spent graphite anodes. The detrimental solid–electrolyte interphase (SEI) is converted to carbon coating, and the spent graphite particle is recrystallized. **e**, Upcycling of waste carbon-fibre-reinforced plastics (CFRP) and waste glass-fibre-reinforced plastics (GFRP) into silicon carbide (SiC) and graphene. In the first step, waste CFRP and GFRP are ground and mixed; in the second step, the mixture is converted to SiC by flash carbothermic reaction. Panel **a** adapted from ref. 36, CC BY 4.0. Panel **e** adapted from ref. 22, Springer Nature Limited.

Coulombic efficiency, superior to commercial graphite[141]. A similar strategy was applied to regenerate spent cathode carbon blocks of aluminium electrolytic cell[142]. In addition to anode regeneration, FJH can achieve the direct recycling of cathodes, such as the relithiation of $LiCoO_2$ and repair of its crystal structure[143]. FJH was also combined with magnetic separation and solid-state relithiation to restore fresh cathodes from waste cathodes, with battery metal recovery yields of ~98% (ref. 144).

Upcycling inorganic wastes into value-added materials. Recycling inorganic wastes that are less valuable than critical metals, such as glass and silicon, is often less profitable. As a result, these waste streams are usually directly landfilled instead of recycled. However, similar to its application in the synthesis of inorganic materials, FJH can be used to convert inorganic waste to value-added inorganic materials. As low-value materials often constitute a major part of inorganic wastes, their upcycling by FJH represents a promising path toward their secondary utilization.

For example, FJH has been used to upcycle glass-fibre-reinforced plastics into silicon carbide[22], a high-performance reinforcement and semiconducting material. Waste glass-fibre-reinforced plastics

were mixed with waste carbon-fibre-reinforced plastics as conductive additives (Fig. 4e). FJH rapidly converted the glass fibre to SiC by carbothermic reduction (Fig. 4e). The phase of SiC can be controlled by the FJH process, similar to the phase-controlled synthesis of molybdenum carbides[15]. The SiC powder obtained was further used as an anode for lithium-ion batteries[22]. In another example, the rapid Joule heating process converts photovoltaic silicon waste into silicon nanowire electrodes for lithium-ion batteries[134].

Carbonaceous waste upcycling

FJH production of graphene was initially optimized with amorphous carbon and coal[11], but many other low-value carbonaceous waste streams[33] have been upcycled into graphene via FJH. Upcycling carbonaceous waste into high-value products such as graphene can economically incentivize the responsible disposal and recovery of resources[145]. The value of the product required to offset process costs is dependent on the demonstrated application, and several promising pathways are discussed here.

Upcycling of waste plastics and rubbers into flash graphene. FJH can be used to upcycle waste plastics[33] and other petrochemical wastes, such as rubber[45], pyrolysis ash[146] and asphaltenes[34]. For example, mixed plastic wastes have been converted to graphene via FJH in a process that does not require sorting or washing (which involves high process costs)[33]. Graphene derived from waste plastics has been tested in applications of lubricants[68], automotive composite applications[12], 3D printing and corrosion resistance[34], and electromagnetic field absorption[147]. Graphene derived from coal has been used as a total substitute for concrete aggregates, producing concrete that is 25% lighter and has superior mechanical properties[67].

Because of the resistive heating nature of FJH, samples must be conductive enough to support the rapid discharge of current required to achieve high temperatures during the process. As waste plastics are not conductive enough, conductive additives are needed. Typically, 10–20 wt% of conductive additives, such as carbon black, tyre-carbon black, charcoal or coal, can be added to reduce the resistance to <10 Ω; however, this can be a costly additive when processing waste streams. A two-step FJH strategy has been developed to use as little as 2–3 wt% of carbon black in the conversion of ground waste plastics into graphene[12] (Fig. 5a). In this two-step method, a longer-duration (10-s), lower-current discharge is conducted to carbonize the carbonaceous feedstock, increasing the conductivity of the material and resulting in volatile outgassing. After this low-current FJH, where some volatile mass is lost dependent on feedstock, the sample resistance is <10 Ω, allowing high-current FJH to occur, as shown in the graph of current versus time in Fig. 5a. Raman spectroscopy shows defective graphitic structure after low-current FJH, which is then annealed into high-quality turbostratic graphene after high-current FJH (Fig. 5b). The carbon black additives are simultaneously converted to graphene, so their separation is not required[12].

The longer heating duration of the two-step FJH process allows alternative products to be synthesized. For example, the incorporation of <1 wt% salts such as $FeCl_3$ catalysed the formation of 1D carbon nanotubes and nanofibres with controllable diameters. By parameter tuning, hybrid morphologies of graphene domains embedded with 1D nanofibres were also produced, which resulted in superior composite mechanical properties when tested in epoxy composites[14]. The incorporation of calcium salts can also function as blowing agents and proppants to increase and maintain the specific surface area during the FJH process. Through the evolution of gases, porosity and wrinkles can be included in the material, resulting in holey, wrinkled flash graphene[76].

Upcycling of waste plastics into hydrogen and chemicals. Carbonization occurs during the low-current FJH of plastics, forming hydrocarbon volatiles including substantial proportions of H_2 gas (Fig. 5c). High yields of H_2 were observed regardless of plastic type (Fig. 5d), with lower initial sample resistances resulting in more complete hydrocarbon breakdown to form higher yields of H_2 and flash graphene. Hydrogen efficiencies as high as 93% were observed, and no CO_2 is produced during the FJH of polyolefins. Compared with traditional pyrolysis[26], the higher heating rate of FJH results in a substantially different product distribution (90 vol% H_2). FJH is, therefore, a catalyst-free method to produce clean H_2 from mixed waste plastics, with the costs potentially offset by the co-production of high-value graphene.

Depolymerization is another widely adopted strategy for waste plastic upcycling[148]. An electrified spatiotemporal heating process based on the rapid Joule heating technique has been tested in the pyrolysis of commodity plastics[149]. This catalyst-free, far-from-equilibrium thermochemical depolymerization method promotes depolymerization while suppressing unwanted side reactions, leading to high-yield monomer recovery: 36% for polypropylene and 43% for poly(ethylene terephthalate). H-ZSM-5 was later introduced as a catalyst to efficiently deconstruct polyolefin plastic wastes into light olefins C_2–C_4 (ref. 150). In that demonstration, the pulsed current input was critical for producing a narrow distribution of gaseous products.

Upcycling of biomass into flash graphene. Although thermal conversion of biomass to biochar has been widely adopted[151], the conversion of biomass to high-value carbon materials such as graphene represents a value-added upcycling route. Biomass such as sawdust and straw[152], lignin[147], waste food[11], hair[46] and even mixed municipal waste[49] can be upcycled into graphene by FJH. No catalyst is required. However, biomass is not conductive, so a conductive additive such as carbon black is required. The biomass usually contains a high oxygen content, such that massive pyrolytic volatiles are released during the FJH process, which accounts for 60–70% of carbon emissions[152]. A two-step process has been developed to allocate energy efficiently[37] and address these emissions. Initially, pyrolysis is used to release biomass pyrolytic volatiles; subsequent FJH reaction is carried out to optimize the flash graphene structure (Fig. 5e). An integrated automatic FJH system has also been built (Fig. 5f), enabling the continuous production of biomass-derived graphene at the productivity of 21.6 g h^{-1} (ref. 37).

Environmental remediation

Environmental remediation processes, such as thermal treatment, thermal desorption and high-temperature vitrification, can have high energy usage and by-products. Improving energy efficiency, reducing by-product emissions and using renewable energy are key research areas toward sustainability in environmental remediation[153]. Owing to its versatility, energy efficiency, widely tunable temperature range (up to 3,000 °C) and lack of secondary waste, FJH has been applied in environmental remediation, including as a thermal process for the decontamination of hazardous wastes and remediation of soil, and in material synthesis for pollution degradation, as discussed in the following sections.

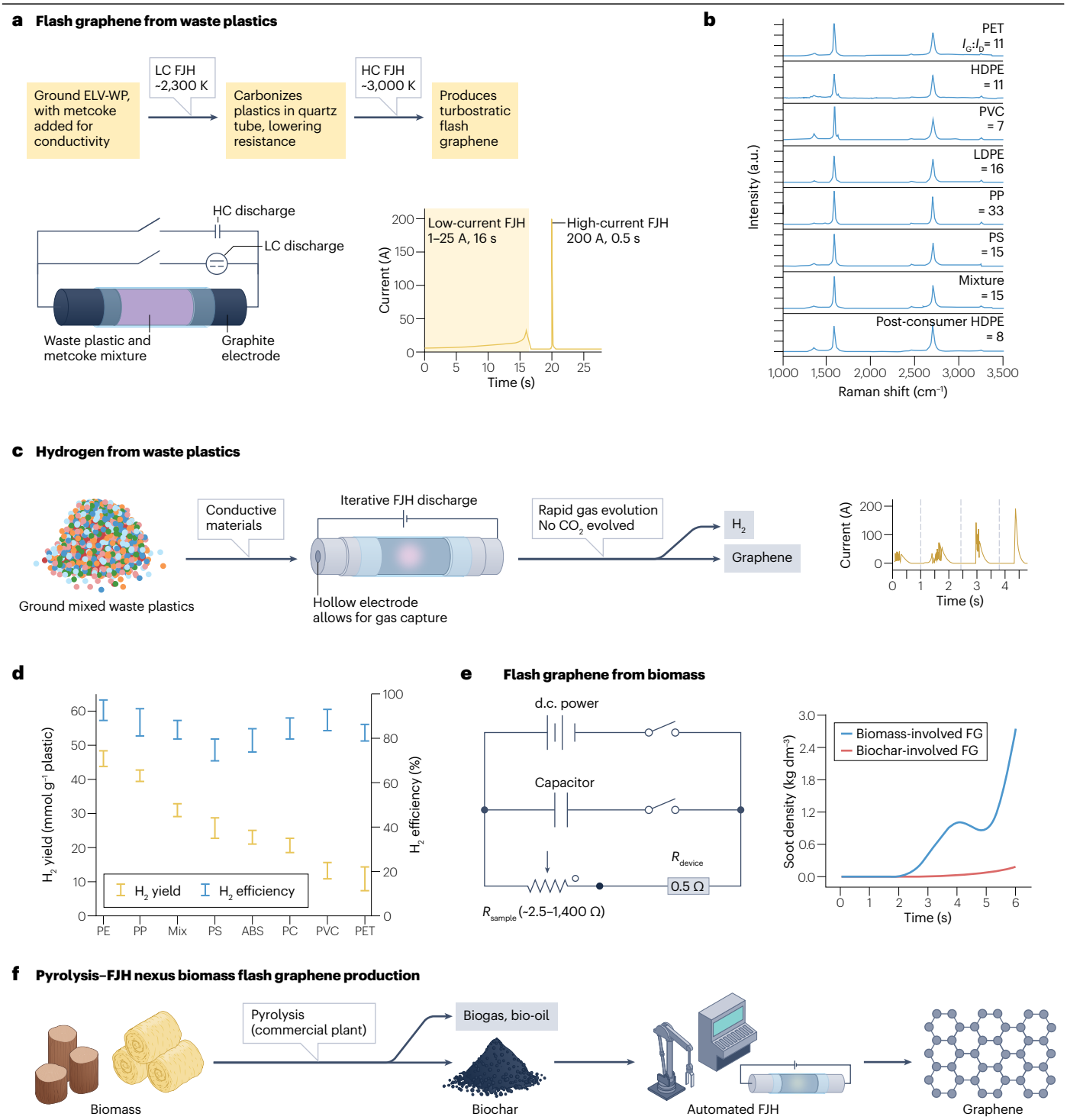

Decontamination of hazardous wastes

Thermal treatment is widely used in hazardous waste decontamination and environmental remediation[153,154]. FJH can achieve a wide temperature range, which is sufficient to degrade organic pollutants and remove heavy metals by evaporation. Heavy metals (including Cd, As, Pb, Ni and Co) have high vapour pressure (Fig. 6a), enabling their evaporative removal with efficiencies of 70–90% at temperatures just below 3,000 °C. For example, during the urban mining of precious metals by FJH, toxic heavy metals, such as Hg, As, Cd, Pb and Cr, are removed by evaporation and then captured by condensation[36]. The heavy metal

Fig. 5 | Upcycling of waste plastics and biomass into flash graphene and clean hydrogen. Flash Joule heating (FJH) can be used to upcycle waste (such as mixed plastics) and biomass. **a**, Conversion of mixed, contaminated end-of-life waste plastics into turbostratic graphene through a two-step FJH process. The example here includes end-of-life vehicle waste plastic (ELV-WP), low-current (LC) and high-current (HC) FJH. The current versus time graph demonstrates the low-current and high-current steps of the FJH conversion of plastics into graphene. **b**, Raman spectra showing the upcycling of various polymer feedstocks into graphene after the high-current FJH process. **c**, Typical FJH process used to convert waste plastics into hydrogen, with the inset graph showing the current discharge as a function of time over four iterative FJH treatments. **d**, H_2 yield and efficiency from FJH synthesis varies by waste plastic type. Error bars represent the standard deviation where $N = 3$. **e**, The equivalent circuit diagram of direct-current FJH system (left), and the soot density of biomass and biochar-involved flash graphene production during FJH (right). **f**, A conceptual design of industrial process for biomass flash graphene production. ABS, acrylonitrile butadiene styrene; FG, flash graphene; HDPE, high-density polyethylene; LDPE, low-density polyethylene; PC, polycarbonate; PET, poly(ethylene terephthalate); PP, polypropylene; PS, polystyrene; PVC, polyvinyl chloride. Panel **a** reprinted from ref. 12, CC BY 4.0. Panel **b** adapted with permission from ref. 33, ACS. Panels **c** and **d** adapted with permission from ref. 26, Wiley. Panel **e** adapted from ref. 37, CC BY 4.0.

content in the residual waste is reduced to within safe limits after two to three FJH pulses under 120 V FJH. Heavy metals in coal fly ash[155] have also been removed during treatment with FJH (Fig. 6a), allowing the purified coal fly ash to be used as a low-carbon cementitious material with reduced heavy metal leaching[155]. FJH has also been used to recycle hazardous zinc-enriched hyperaccumulators into graphitic materials while removing 98.6% of the zinc[156].

FJH has been shown to be an effective technique for the electrothermal mineralization of PFAS[157]. A common strategy to remove PFAS in water is adsorption, using sorbent-like granular activated carbon[158]. Traditional thermal methods for treatment of this PFAS-contaminated carbon, such as incineration, are energy intensive and can release hazardous gaseous fluorocarbons; they therefore require secondary flame scrubbers to mitigate the gaseous release[159]. In the presence of sodium or calcium hydroxides, PFAS sorbed on granular activated carbon are converted into non-toxic fluoride salts by FJH (Fig. 6b). High fluorine conversion efficiencies of >96% are achieved within 1 s, with undetectable gaseous fluorocarbons, and it is much faster than traditional incineration[157].

Soil remediation

Thermal desorption[153], such as in thermal conduction heating and electrical resistive heating, is a practical method for soil remediation. Traditional thermal desorption technologies usually operate at temperatures <500 °C, so they are only suitable for the remediation of volatile or semivolatile contaminants[160]. FJH can be applied to soil remediation to remove multiple pollutants simultaneously[25]: heavy metals are removed by evaporation, while persistent organic pollutants such as polycyclic aromatic hydrocarbons are removed by carburization (Fig. 6c).

Compared with conventional thermal techniques, the electrothermal remediation processes are much faster, within seconds rather than days or even months, and they have higher degradation capability for pollutants[25]. For example, the removal efficiencies of tested heavy metals such as Cd, Hg and Pb were >80% in a single FJH pulse[25]; the degradation degrees of tested polycyclic aromatic hydrocarbons including pyrene, fluorene and benz[*a*]anthracene were >93% in three FJH pulses[25]. The high-temperature electrothermal process of FJH can potentially be integrated with vapour extraction pipes for in situ remediation[25]. However, in contrast to traditional electrical resistance heating techniques that rely on the thermal conductivity and slow heat diffusion of the soil itself, in the FJH process, premixing conductive carbon (such as biochar) soil particles is required to provide sufficient conductivity for the Joule heating. The conductive additives can be recycled by mechanical sieving based on the size differences between the soil and the carbon additives and then reused to minimize the materials consumption of the remediation process[25]. Currently, FJH for soil remediation has been demonstrated on a laboratory scale; further field tests are required to assess the soil properties.

FJH has also been used for the remediation of PFAS in soil at the kilogram scale[24] (Fig. 6d). With biochar as a conductive additive, FJH is used to ramp the soil temperature to >1,000 °C in seconds. PFAS then reacts with in situ calcium compounds to form calcium fluorides and other alkaline earth fluorides, which are non-toxic and the natural mineralized form of fluoride in the environment. High PFAS removal efficiencies of >99% have been achieved with this method without the use of any external reagents. The soil retains most of its physicochemical properties after the FJH remediation process[25,79]. This method is a proof-of-concept work at the bench scale, and further scaling up is required to assess its applicability and economic viability at larger scales.

Functional materials for pollutant degradation and removal

Environmental catalysis for pollutant degradation can be synthesized via FJH without producing secondary waste during their synthesis. For example, iron-based material is one of the most important catalysts for the advanced oxidation process to degrade organic pollutants in wastewater[161]. With soft carbon as the conductive additive, FJH was used to transform a low-grade, inexpensive FeS mineral into nanoscale Fe(0)/FeS heterostructures embedded in thin graphene layers[108]. With $Fe(NO)_3$ as a precursor, Fe single atoms and nanoparticles were also produced[109]. These materials catalysed an advanced oxidation process for chloramphenicol degradation[108,109]. For example, the Fe-based materials show a chloramphenicol removal efficiency of >94% via catalytic activation of sodium peroxydisulfate[108]. FJH was also applied to synthesize carbon-coated Mg(0)/MgO, which is used in activating peroxydisulfate to degrade sulfamethoxazole, an antibiotic present in wastewater[162].

In addition to acting as catalysts for oxidation processes, low-valent or zero-valent metals are promising for reductive remediation[163]. During FJH synthesis, a carbon layer is coated on the Fe(0) nanoparticle, which prevents its surface oxidation[164]. This Fe–C composite demonstrates superior reductive remediation of multiple pollutants in wastewater, such as water-soluble PFAS, Cr(VI) and Sb(V). By further incorporating Mg with the Fe, a reductive Fe–Mg bimetallic nanocomposite can be synthesized using FJH[165]. This composite leads to the efficient removal of heavy metals from wastewater, including Cr(VI), Sb(V), Ni(II) and Cu(II), with a 2–3 times increase in efficiency compared with monometallic composites.

FJH can also produce the materials for the removal of volatile organic compounds, such as carbon-supported Ag–Co_3O_4 bimetallic

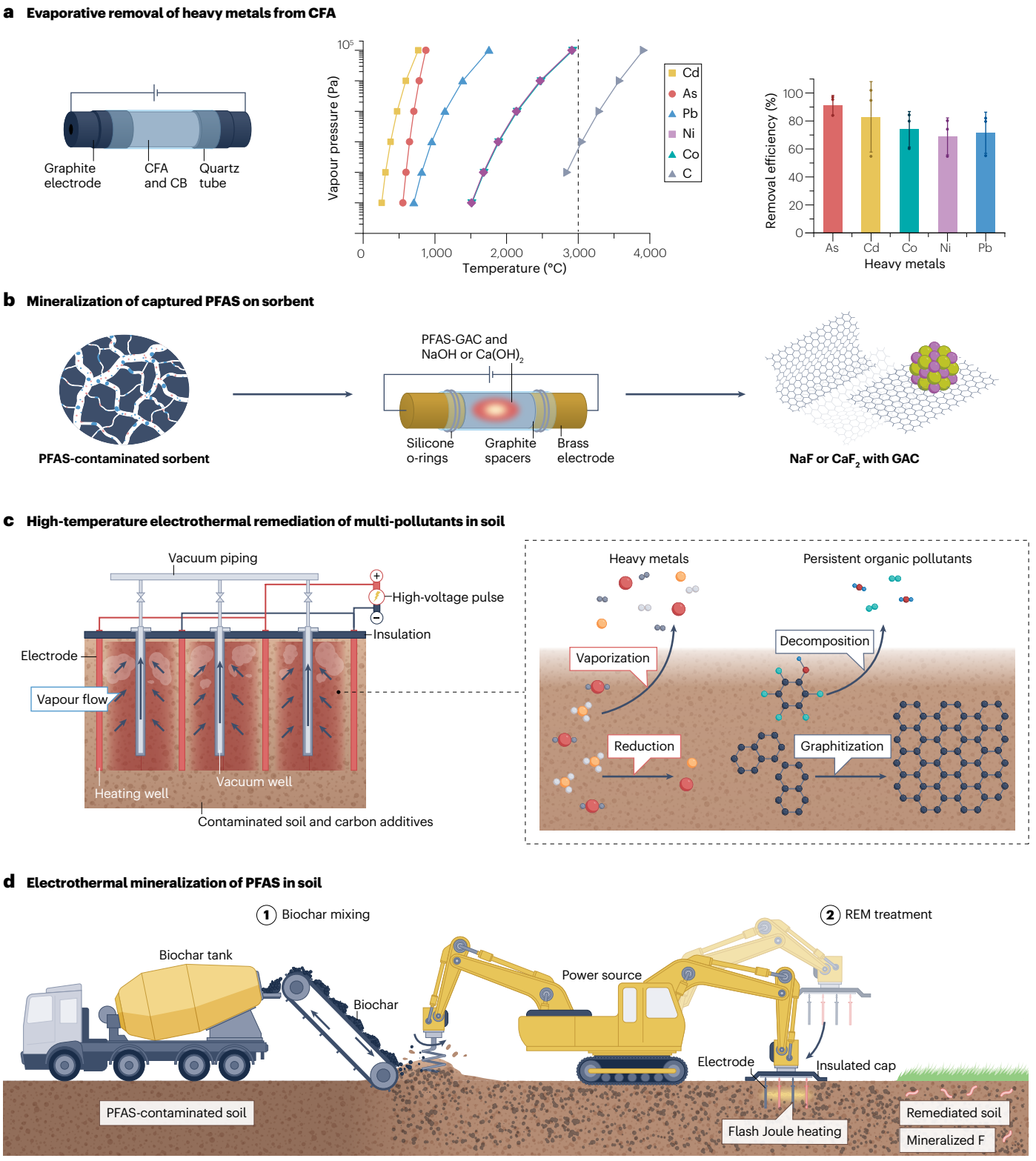

catalyst for the catalytic oxidation removal of formaldehyde[166]. In another example, Joule heating serves as the thermal source to drive the catalytic oxidation of volatile organic compounds using Pt/CeO_2 as the catalysts. This Joule-heating-based catalytic system exhibits an ultralow input power[167], 87% lower than that of a conventional heating furnace.

Fig. 6 | FJH for waste decontamination and soil remediation. Flash Joule heating (FJH) can be used in waste decontamination and soil remediation instead of or in addition to conventional processes. **a**, The removal of heavy metals from coal fly ash (CFA, left), vapour pressure of different heavy metals (centre) and their removal efficiencies by FJH (right). **b**, FJH process for degradation of perfluoroalkyl and polyfluoroalkyl substances (PFAS), in which PFAS adsorbed on granular activated carbon (GAC) is mixed with a metal hydroxide (NaOH or $Ca(OH)_2$). FJH converts the PFAS into non-toxic NaF or CaF_2. **c**, The high-temperature electrothermal process enabled by FJH for soil remediation. The soil is premixed in place, with biochar or other conductive carbon to provide sufficient conductivity. The electrodes provide a rapid voltage pulse for Joule heating, carbonizing the organic pollutants and reducing and vaporizing heavy metals, which are removed by the vacuum piping system. **d**, Electrothermal mineralization for bulk soil remediation of PFAS contaminants. REM is rapid electrothermal mineralization, an FJH process within soil. CB, carbon black. Panel **a** adapted from ref. 155, CC BY 4.0. Panel **c** adapted from ref. 25, CC BY 4.0.

Sustainability and technoeconomic considerations

Quantifying resource use and waste emissions throughout the production, use, or disposal aspects of the FJH allows for direct comparison of different methods. Life-cycle assessment (LCA) and technoeconomic analysis (TEA) have been used to understand the impacts of FJH. These assessments indicate that the high efficiency, short duration, solvent-free nature and minimal heat loss of FJH processes result in substantial reductions in emissions and energy consumption compared with radiative heating or wet-chemistry methods. However, the maximum scales of the processes differ, so there is some uncertainty. This section examines the sustainability of graphene production and waste management using FJH and notes the limitations of these approaches.

Graphene and inorganic materials production

LCA typically includes raw material and resource extraction, which can have high environmental burdens. These impacts can be minimized or even eliminated when using waste feedstocks for flash graphene and other material synthesis by FJH (Fig. 7a), as it requires no graphite mining or solvents in processing. Using waste materials, such as pyrolysis ash[146], waste plastics[12,14], waste printed circuit boards[36], e-wastes[136], retired wind turbine blades[22], coal fly ash[155] and spent rechargeable batteries[132], as feedstocks has provided a substantial reduction in energy intensity and emissions for many FJH processes.

For example, production of flash graphene from end-of-life vehicles has been compared with two common, commercially scaled production methods including graphite exfoliation by sonication or chemical oxidation and reduction, based on a functional unit of 1 kg of graphene powder produced (Fig. 7b–d). There was a substantial reduction in the required co-feedstocks owing to the use of waste materials, and the FJH process overall resulted in >80% reductions in all burdens including greenhouse gas emissions, cumulative energy demand, and water use (Fig. 7b–d). Similarly, the FJH process for upcycling waste biomass into flash graphene results in ~90% reduction in the environmental footprint, especially carbon emissions and freshwater use, when compared with traditional production processes like electrochemical exfoliation[152]. FJH synthesis of other graphitic nanomaterials, such as carbon nanotubes and nanofibres, also has an 86–94% reduction in emissions and energy demand versus conventional production methods[14]. Similar results were observed for transition-metal dichalcogenide production compared with current production methods[20].

In solid-state syntheses, FJH competes primarily with chemical exfoliation[168], chemical vapour deposition[169,170], and electrochemical intercalation[171] (Fig. 7e). Chemical vapour deposition and exfoliation methods require expensive feedstock costs, long reaction times and high energy usage, and low reaction yields are typical[170]. In contrast, FJH has short reaction times and can use low-cost or waste feedstocks with minimal waste by-products, so there can be a substantial decrease in the production cost of flash graphene and related products[49,152]. A TEA of preparation shows that flash graphene can be made at US$0.16 kg^{-1}, markedly lower than the ultrasonication of graphite and reduction of graphene oxide[23], which costs up to US$44 kg^{-1}. Similarly, a preliminary product cost of 2D materials synthesis shows that the FWF FJH offers large cost savings over other synthesis methods, such as autoclave and chemical vapour transport[20]. For example, it takes ~US$600 to synthesize 100 g of $MoSe_2$ materials by FWF FJH, whereas this number can be up to ~US$4,500 by chemical vapour transport[20].

Waste upcycling and decontamination

The application of FJH for metal recovery, waste decontamination and environmental remediation has advantages relative to various widely used methods, based on LCA and TEA. For example, the recycling of battery cathode metals by FJH has reduced water consumption, energy usage, greenhouse gas emissions and costs compared to virgin mining, hydrometallurgical processing, and pyrometallurgical processing[132] (Fig. 7f-h). Similarly, compared to synthetic graphite production and high-temperature calcination recycling[133], the flash recycling of graphite anode materials had substantial reductions in water and energy consumption and greenhouse gas emissions. These reductions were attributed to the rate and energy efficiency of the FJH process. The environmental impacts and costs of upcycling plastic-reinforced glass fibre by FJH have also been compared with other approaches[22]. The operating cost of FJH was equivalent to ~0.2% and ~3.4% of the solvolysis and incineration processes, respectively, to recycle the same amount of waste plastic-reinforced glass fibre and produce the same amount of silicon carbides.

FJH seems to be economically feasible and a viable approach to waste decontamination and environmental remediation. In an LCA of heavy metal removal from coal fly ash by FJH and its reuse in cement[155], there was a 30% reduction in greenhouse gas emissions compared with direct landfilling of the coal fly ash. These results indicate that the coal fly ash can be used as a lower-carbon-footprint cement. A TEA of FJH in soil remediation demonstrated that the electrothermal remediation process shows a 5–70% reduction in operating expenses relative to the different established methods, such as thermal desorption, soil washing and chemical oxidation, that are used at the industrial scale[25]. Similar analyses have been conducted on electrothermal PFAS mineralization by FJH[24,157], showing its substantial reduction in energy consumption, greenhouse gas emissions, water consumption and operation costs when compared with existing methods such as incineration, ball milling and chemical oxidation.

Limitations of current LCA and TEA

As with all preliminary LCA and TEA, the current analyses of the FJH process have limitations. These include assumptions or omissions regarding scalability, transportation, waste feedstock availability and cost, as well as disposal of waste by-products. Widespread adaptation

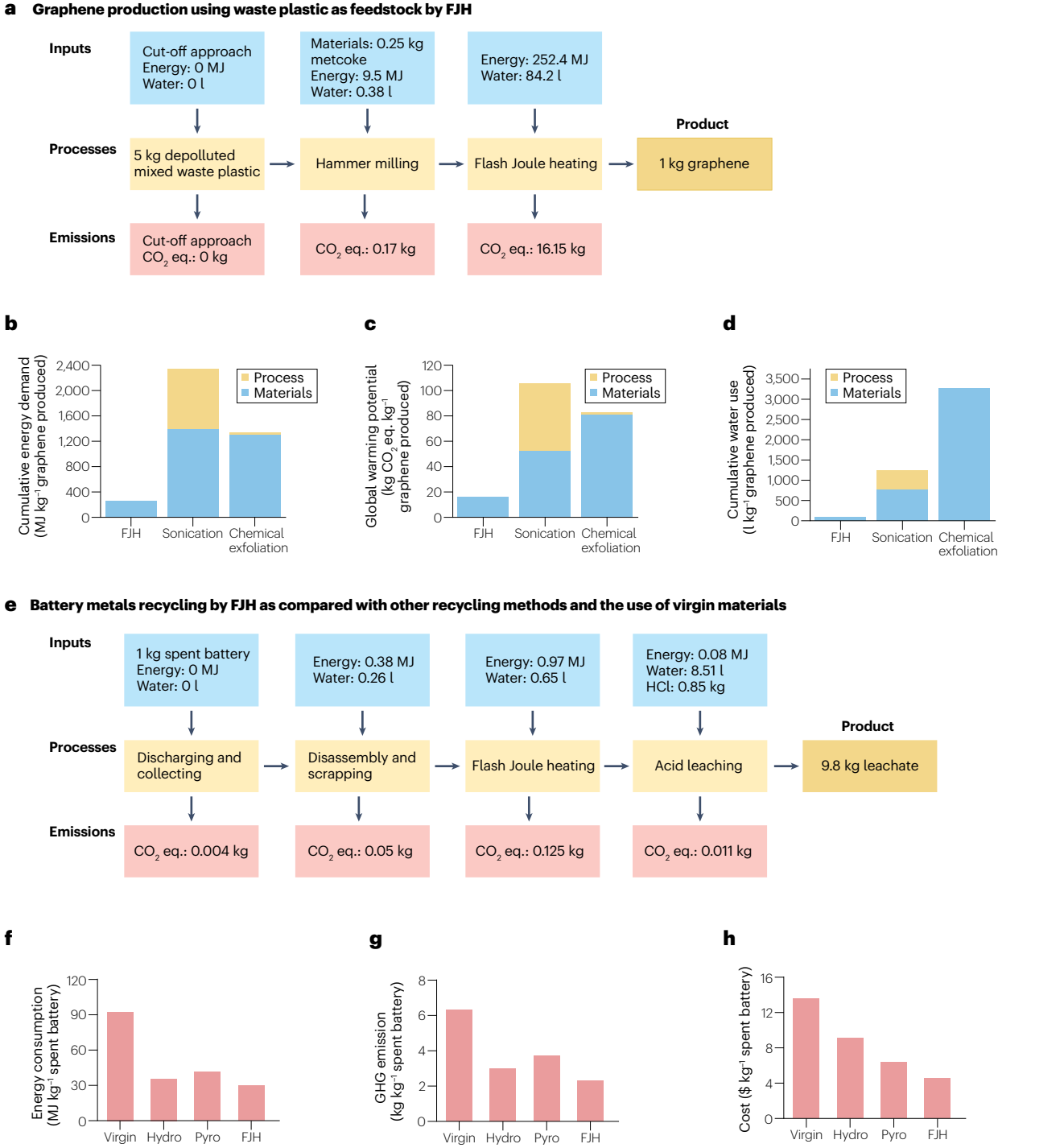

Fig. 7 | Life-cycle assessment and technoeconomic analysis of processes conducted by FJH. Flash Joule heating (FJH) shows promise in life-cycle assessment (LCA) and technoeconomic analysis, offering reduced energy consumption, emissions and costs compared with traditional processes. **a**, Process flow diagram of graphene production using waste plastic as feedstock by FJH. The cut-off approach disregards burdens associated with waste products, such as waste plastics, as these burdens can be attributed to the objects' primary use. **b**–**d**, LCA comparing the FJH method of graphene production from waste plastics with other commercialized graphene production methods including cumulative energy demand (panel **b**), global warming potential (panel **c**) and cumulative water use (panel **d**). **e**, Process flow diagrams of spent lithium-ion battery recycling by FJH activation and acid leaching. **f**–**h**, LCA and technoeconomic analysis of the FJH battery metal recycling process as compared with the use of virgin battery metals, hydrometallurgical method (hydro) and pyrometallurgical method (pyro), including energy consumption (panel **f**), greenhouse gas (GHG) emissions (panel **g**) and cost (panel **h**). CO_2 eq., CO_2 equivalent. Panels **a**–**d** adapted from ref. 12, CC BY 4.0. Panels **e**–**h** adapted from ref. 132, CC BY 4.0.

Glossary

Ceramic sintering
A process of compacting solid materials that results in a more durable, stronger and harder mass, owing to pressure and high heat that force the atoms to bond more tightly with each other.

Critical metals
A group of metals that are vital to high-tech applications, such as rare earth metals, but whose secure supply is potentially at risk of restriction.

Dielectric heating
The process in which a radiofrequency alternating electric field, radio wave or microwave electromagnetic radiation heats a dielectric material.

Direct heating
The process of transferring heat directly to a target material without using an intermediary fluid or medium. The heat source is in direct contact with the target, or the heat is generated inside the target itself.

Electric arc heating
An electrothermal process in which an electric arc is formed between two electrodes, generating high temperatures.

Flash graphene
The turbostratic graphene produced by the flash Joule heating process.

Flash Joule heating
A resistive heating process that uses pulsed current passing through the target material to rapidly heat it to a high temperature directly followed by ultrafast cooling.

Flash sintering
A sintering technology that involves the application of a direct electrical field via customized electrodes to a material body during the sintering process.

Indirect heating
The process of transferring heat to a target materials through an intermediate.

Induction heating
The process of heating electrically conductive materials by electromagnetic induction, in which heat transfer passing through an inductor that creates an electromagnetic field within the coil to heat up.

Life-cycle assessment
A methodology for assessing environmental impacts associated with all stages of the life cycle of a product, process or service.

Metastability
An intermediate energetic state within a dynamical system other than the system's state of least energy.

Metastable materials
Materials that have metastable phases with kinetically trapped states with positive free energy above the thermodynamically equilibrium state; these phases can exhibit unique properties compared with their stable counterparts.

Ordered graphene
Ordered graphene refers to graphene that exhibits a high degree of structural organization, typically in terms of its atomic arrangement, stacking or alignment. It implies a regular and well-defined crystalline structure, as opposed to disordered or amorphous forms of graphene.

Perfluoroalkyl and polyfluoroalkyl substances
A group of synthetic organofluorine chemical compounds that have multiple fluorine atoms attached to an alkyl chain.

Solid-state synthesis
A method used to produce materials by reacting solid-phase precursors without involving a liquid or gaseous medium; this process typically involves heating the solid reactants to a high temperature to facilitate the reaction.

Spark plasma sintering
A ceramic sintering process involving the application of pulsed direct current and uniaxial pressure to the powder within a die.

Technoeconomic analysis
A method of analysing the economic performance of an industrial process, product or service.

Upcycling
The process of transforming by-products, waste materials, useless or unwanted products into new materials or products perceived to be of greater quality or higher value.

Urban mining
The extraction of valuable materials, such as metals, from discarded urban materials, particularly electronic wastes.

Variable frequency drive
A type of a.c. motor drive that controls speed and torque by varying the frequency of the input electricity.

of sustainable technologies based solely on top-line, preliminary LCA and TEA data might result in over-estimation of environmental benefits or efficiency improvements, owing to altered consumption behaviours[172,173]. This rebound effect in the circular economy is a result of projected efficiency gains of new sustainable technology being unrealized, owing to increased consumption of goods once the technology has reached large scales[174].

As many of the published LCAs conducted on the FJH processes are preliminary in scope and make assumptions about scale and adoption, most do not consider rebound effects. For example, a lower cost of graphene would logically result in increased consumption, which could result in an overall increase in burdens and footprint attributable to the graphene market, even with the improved efficiency of the FJH process. This would be a direct rebound effect, but indirect rebound effects could also be observed in which the increased efficiency and lowered cost might result in an increased prevalence of unrelated manufacturing processes, such as increased cathode production due to the implementation of cheaper anode recycling. Both direct and indirect rebound effects can be difficult to predict, and they also apply to TEA, not only to LCA projections[175]. Further examples of rebound effects include the increased demand for biomass-derived FJH graphene, resulting in higher overall biomass consumption and thus greater land use burdens or increased emissions from transportation.

Scientists can help to acknowledge these possibilities by conducting thorough uncertainty analysis in LCA and TEA, as well as considering a wide array of scenarios, including process energy sources, materials transportation, and comparison to associated primary production routes that might have increased use rather than a decline in use[176]. Furthermore, detailed LCA and TEA with a broader scope, using different assumptions, comparing different methods or analysing different scale FJH processes, can enhance the quantified understanding of cost and burden efficiency. Overall, conducting LCA and TEA during the early stages of FJH developments, optimization and scale-up can help to identify steps of high burden, as well as benchmark or suggest the sustainability in quantifiable terms.

Summary and future perspectives

FJH has emerged as an efficient electrification technology for materials production, metal recycling, waste upcycling and environmental remediation. Its hallmark features, including high energy efficiency, short reaction duration, solvent-free processing, minimal heat loss, versatile operation models and compact reactor design, provide advantages over traditional combustion-based heating or wet-chemistry methods. Despite progress in the development and application of FJH, efforts are needed to elucidate the underlying mechanisms, better harness its characteristics and advance FJH toward industrial-scale implementation.

More experimental and theoretical analyses are needed to uncover the mechanism and improve the controllability of FJH. Advanced characterization under realistic in operando reaction conditions will be necessary to clarify the reaction and conversion details[177]. FJH is a multi-physical phenomenon that combines electric fields, thermal fields, and intense light emission. A comprehensive understanding of the multifield coupling effect is crucial for enhancing its controllability. Further, improving temperature control is necessary for better uniformity of the reaction conversions.

FJH complements existing heating techniques, such as furnace heating, microwave heating and induction heating. Its differences from these techniques offer new possibilities for researchers working in diverse disciplines applications, as demonstrated by the successful application of FJH in materials production, chemical syntheses and environmental remediation. In particular, few applications in wet chemistry and gas reactions have been reported, but these warrant further investigation as the ultrafast and highly localized heating of FJH could offer distinct kinetic and thermodynamic advantages over traditional heating methods. FJH for waste recycling and environmental remediation also requires more detailed comparative studies than established methods before deployment.

The scale-up of the FJH process and its industry-scale implementation and automation are pivotal to realizing its use in energy-efficient applications. The prototype productivity of flash graphene production had been reported at larger scales, but the FJH synthesis of inorganic materials is at the gram-scale level in the laboratory. Ideally, lessons on scalable FJH technology in graphene production can be adapted for the mass production of other materials. Scale-up is also needed for waste recycling and environmental remediation, given the quantities of solid waste generated. For instance, coal power plants currently produce >750 million tonnes of fly ash per year[178]. For further scale-up, the electricity supply system needs design upgrades to ensure high and rapid power input[41]. For pilot-scale or industrial implementation of FJH, waste heat recovery and off-gas treatment systems should be integrated into FJH systems, allowing heat and gas to be recovered from the FJH process. This design requires collaboration between academia and industry to bring FJH into large-scale practice.

Published online: 15 January 2025

References

1. Deshmukh, Y. V. *Industrial Heating: Principles, Techniques, Materials, Applications, and Design* 1st edn (CRC, 2005).
2. Hasanuzzaman, M. et al. Energy savings in the combustion based process heating in industrial sector. *Renew. Sustain. Energy Rev.* **16**, 4527–4536 (2012).
3. Sugiyama, M. Climate change mitigation and electrification. *Energy Policy* **44**, 464–468 (2012).
4. Global CO_2 emissions by sector, 2019–2022. *IEA* https://www.iea.org/data-and-statistics/charts/global-co2-emissions-by-sector-2019-2022 (2022).
5. Wei, M., McMillan, C. A. & de la Rue du Can, S. Electrification of industry: potential, challenges and outlook. *Curr. Sustain./Renew. Energy Rep.* **6**, 140–148 (2019).
6. Fryer, P. & Li, Z. Electrical resistance heating of foods. *Trends Food Sci. Technol.* **4**, 364–369 (1993).
7. Toulouevski, Y. N. & Zinurov, I. Y. in *Innovation in Electric Arc Furnaces: Scientific Basis for Selection* (eds Toulouevski, Y. N. & Zinurov, I. Y.) 1–24 (Springer, 2013).
8. Lucía, O., Maussion, P., Dede, E. J. & Burdío, J. M. Induction heating technology and its applications: past developments, current technology, and future challenges. *IEEE Trans. Ind. Electron.* **61**, 2509–2520 (2014).
9. Gabriel, C. et al. Dielectric parameters relevant to microwave dielectric heating. *Chem. Soc. Rev.* **27**, 213–224 (1998).
10. Wismann, S. T. et al. Electrified methane reforming: a compact approach to greener industrial hydrogen production. *Science* **364**, 756–759 (2019).
11. Luong, D. X. et al. Gram-scale bottom-up flash graphene synthesis. *Nature* **577**, 647–651 (2020).
12. Wyss, K. M. et al. Upcycling end-of-life vehicle waste plastic into flash graphene. *Commun. Eng.* **1**, 3 (2022).
13. Huang, P., Zhu, R., Zhang, X. & Zhang, W. Effect of free radicals and electric field on preparation of coal pitch-derived graphene using flash Joule heating. *Chem. Eng. J.* **450**, 137999 (2022).
14. Wyss, K. M. et al. Upcycling of waste plastic into hybrid carbon nanomaterials. *Adv. Mater.* **35**, 2209621 (2023).
15. Deng, B. et al. Phase controlled synthesis of transition metal carbide nanocrystals by ultrafast flash Joule heating. *Nat. Commun.* **13**, 262 (2022).
16. Taibi, A., Gil-González, E., Sánchez-Jiménez, P. E., Perejón, A. & Pérez-Maqueda, L. A. Flash Joule heating-boro/carbothermal reduction (FJH-BCTR): an approach for the instantaneous synthesis of transition metal diborides. *Ceram. Int.* https://doi.org/10.1016/j.ceramint.2024.01.144 (2024).
17. Shen, P. et al. General synthesis of transition metal nitride arrays by ultrafast flash joule heating within 500 ms. *Sci. China Chem.* **67**, 1976–1982 (2024).
18. Deng, B. et al. Kinetically controlled synthesis of metallic glass nanoparticles with expanded composition space. *Adv. Mater.* **36**, 2309956 (2024).
19. Okulov, I. V. et al. Flash Joule heating for ductilization of metallic glasses. *Nat. Commun.* **6**, 7932 (2015).
20. Choi, C. H. et al. Flash-within-flash synthesis of gram-scale solid-state materials. *Nat. Chem.* **16**, 1831–1837 (2024).
21. Chen, W. et al. Heteroatom-doped flash graphene. *ACS Nano* **16**, 6646–6656 (2022).
22. Cheng, Y. et al. Flash upcycling of waste glass fibre-reinforced plastics to silicon carbide. *Nat. Sustain.* **7**, 452–462 (2024).
23. Eddy, L. J. et al. Automated laboratory kilogram-scale graphene production from coal. *Small Methods* **8**, 2301144 (2024).
24. Cheng, Y. et al. Electrothermal mineralization of per- and polyfluoroalkyl substances for soil remediation. *Nat. Commun.* **15**, 6117 (2024).
25. Deng, B. et al. High-temperature electrothermal remediation of multi-pollutants in soil. *Nat. Commun.* **14**, 6371 (2023).
26. Wyss, K. M. et al. Synthesis of clean hydrogen gas from waste plastic at zero net cost. *Adv. Mater.* **35**, 2306763 (2023).
27. Deng, B. et al. Rare earth elements from waste. *Sci. Adv.* **8**, eabm3132 (2022).
28. Joule, J. P. On the production of heat by voltaic electricity. *Proc. R. Soc. Lond.* **4**, 280–281 (1841).
29. Walton, R. R. in *Kirk-Othmer Encyclopedia of Chemical Technology* Vol. 7 16–23 (Wiley, 2000).
30. Eddy, L. et al. Electric field effects in flash Joule heating synthesis. *J. Am. Chem. Soc.* **146**, 16010–16019 (2024).
31. Cheng, Y. et al. Electric current aligning component units during graphene fiber Joule heating. *Adv. Funct. Mater.* **32**, 2103493 (2022).
32. Zhang, X. H., Han, G. Y. & Zhu, S. Flash nitrogen-doped carbon nanotubes for energy storage and conversion. *Small* **20**, 2305406 (2024).
33. Algozeeb, W. A. et al. Flash graphene from plastic waste. *ACS Nano* **14**, 15595–15604 (2020).
34. Saadi, M. A. S. R. et al. Sustainable valorization of asphaltenes via flash Joule heating. *Sci. Adv.* **8**, eadd3555 (2022).
35. Chen, W. et al. Ultrafast and controllable phase evolution by flash Joule heating. *ACS Nano* **15**, 11158–11167 (2021).
36. Deng, B. et al. Urban mining by flash Joule heating. *Nat. Commun.* **12**, 5794 (2021).
37. Zhu, X. et al. Continuous and low-carbon production of biomass flash graphene. *Nat. Commun.* **15**, 3218 (2024).
38. Wang, C. et al. A general method to synthesize and sinter bulk ceramics in seconds. *Science* **368**, 521–526 (2020).
39. Deng, B. et al. High-surface-area corundum nanoparticles by resistive hotspot-induced phase transformation. *Nat. Commun.* **13**, 5027 (2022).
40. Mishra, S. & Ullas, A. V. Concept modelling of small scale device for continuous production of graphene using Solidworks. *Mater. Today Proc.* **79**, 345–348 (2023).
41. Eddy, L. et al. Kilogram flash Joule heating synthesis with an arc welder. Preprint at *ChemRxiv* https://doi.org/10.26434/chemrxiv-2024-nfnc9 (2024).
42. Dwivedi, I. & Subramaniam, C. Joule heating-driven transformation of hard-carbons to onion-like carbon monoliths for efficient capture of volatile organic compounds. *ACS Mater. Au* **2**, 154–162 (2022).
43. Dong, S. et al. Rapid carbonization of anthracite coal via flash Joule heating for sodium ion storage. *ACS Appl. Energy Mater.* https://doi.org/10.1021/acsaem.3c02975 (2024).

44. Liu, X. & Luo, H. Preparation of coal-based graphene by flash Joule heating. *ACS Omega* **9**, 2657–2663 (2024).
45. Advincula, P. A. et al. Flash graphene from rubber waste. *Carbon* **178**, 649–656 (2021).
46. Kaur, J. et al. Sustainable manufacturing of graphitic carbon from bio-waste using flash heating for anode material of lithium-ion batteries with optimal performance. *Adv. Sustain. Syst.* https://doi.org/10.1002/adsu.202300610 (2024).
47. Advincula, P. A., Meng, W., Beckham, J. L., Nagarajaiah, S. & Tour, J. M. Conversion of CO_2-derived amorphous carbon into flash graphene additives. *Macromol. Mater. Eng.* **309**, 2300266 (2024).
48. Teng, T. et al. Flash reforming pyrogenic carbon to graphene for boosting advanced oxidation reaction. *Adv. Mater. Technol.* **8**, 2300236 (2023).
49. Silva, K. J. et al. Graphene derived from municipal solid waste. *Small* https://doi.org/10.1002/smll.202311021 (2024).
50. Cheng, L. et al. Flash healing of laser-induced graphene. *Nat. Commun.* **15**, 2925 (2024).
51. ISO/TS 80004-13:2024(en). Nanotechnologies — vocabulary — part 13: graphene and related two-dimensional (2D) materials. *ISO* https://www.iso.org/obp/ui/#iso:std:iso:ts:80004:-13:ed-2:v1:en (2024).
52. Partoens, B. & Peeters, F. M. From graphene to graphite: electronic structure around the K point. *Phys. Rev. B* **74**, 075404 (2006).
53. Lespade, P., Marchand, A., Couzi, M. & Cruege, F. Caracterisation de materiaux carbones par microspectrometrie Raman. *Carbon* **22**, 375–385 (1984).
54. Deng, B. et al. Interlayer decoupling in 30° twisted bilayer graphene quasicrystal. *ACS Nano* **14**, 1656–1664 (2020).
55. Kokmat, P., Surinlert, P. & Ruammaitree, A. Growth of high-purity and high-quality turbostratic graphene with different interlayer spacings. *ACS Omega* **8**, 4010–4018 (2023).
56. Garlow, J. A. et al. Large-area growth of turbostratic graphene on Ni(111) via physical vapor deposition. *Sci. Rep.* **6**, 19804 (2016).
57. Malard, L. M., Pimenta, M. A., Dresselhaus, G. & Dresselhaus, M. S. Raman spectroscopy in graphene. *Phys. Rep.* **473**, 51–87 (2009).
58. Beckham, J. L. et al. Machine learning guided synthesis of flash graphene. *Adv. Mater.* **34**, 2106506 (2022).
59. Wyss, K. M., Wang, Z., Alemany, L. B., Kittrell, C. & Tour, J. M. Bulk production of any ratio ^{12}C:^{13}C turbostratic flash graphene and its unusual spectroscopic characteristics. *ACS Nano* **15**, 10542–10552 (2021).
60. Seehra, M. S., Geddam, U. K., Schwegler-Berry, D. & Stefaniak, A. B. Detection and quantification of 2H and 3R phases in commercial graphene-based materials. *Carbon* **95**, 818–823 (2015).
61. Stanford, M. G. et al. Flash graphene morphologies. *ACS Nano* **14**, 13691–13699 (2020).
62. Deng, B. et al. Wrinkle-free single-crystal graphene wafer grown on strain-engineered substrates. *ACS Nano* **11**, 12337–12345 (2017).
63. Deng, B. et al. Growth of ultraflat graphene with greatly enhanced mechanical properties. *Nano Lett.* **20**, 6798–6806 (2020).
64. Pang, Z., Deng, B., Liu, Z., Peng, H. & Wei, Y. Defects guided wrinkling in graphene on copper substrate. *Carbon* **143**, 736–742 (2019).
65. Li, F. et al. Ultrafast synthesis of battery grade graphite enabled by a multi-physics field carbonization. *Chem. Eng. J.* **461**, 142128 (2023).
66. Advincula, P. A. et al. Ultra-high loading of coal-derived flash graphene additives in epoxy composites. *Macromol. Mater. Eng.* **308**, 2200640 (2023).
67. Advincula, P. A. et al. Replacement of concrete aggregates with coal-derived flash graphene. *ACS Appl. Mater. Interfaces* **16**, 1474–1481 (2024).
68. Advincula, P. A. et al. Waste plastic- and coke-derived flash graphene as lubricant additives. *Carbon* **203**, 876–885 (2023).
69. Yang, H. et al. Ordered-range tuning of flash graphene for fast-charging lithium-ion batteries. *ACS Appl. Nano Mater.* **6**, 2450–2458 (2023).
70. Chen, Y. et al. Bioinspired robust gas-permeable on-skin electronics: armor-designed nanoporous flash graphene assembly enhancing mechanical resilience. *Adv. Sci.* **11**, 2402759 (2024).
71. Zhou, C. et al. Preparation of graphene-coated Cu particles with oxidation resistance by flash joule heating. *Carbon* **224**, 119060 (2024).
72. Chen, J. et al. Cathode-electrolyte interphase engineering toward fast-charging $LiFePO_4$ cathodes by flash carbon coating. *Small Methods* https://doi.org/10.1002/smtd.202400680 (2024).
73. Zhu, S. et al. Flash nitrogen-doped graphene for high-rate supercapacitors. *ACS Mater. Lett.* **4**, 1863–1871 (2022).
74. Chen, W. et al. Turbostratic boron–carbon–nitrogen and boron nitride by flash Joule heating. *Adv. Mater.* **34**, 2202666 (2022).
75. Cui, P. et al. Enhancing electrochemical performance through swift functional group tuning of MXenes. *Batter. Supercaps* **7**, e202400274 (2024).
76. Wyss, K. M., Chen, W., Beckham, J. L., Savas, P. E. & Tour, J. M. Holey and wrinkled flash graphene from mixed plastic waste. *ACS Nano* **16**, 7804–7815 (2022).
77. Liao, Y. T. et al. Ultrafast synthesis of 3D porous flash graphene and its adsorption properties. *Colloid Surf. A* **676**, 132178 (2023).
78. Li, Q. et al. Rapid preparation of porous carbon by flash Joule heating from bituminous coal and its adsorption mechanism of methylene blue. *Colloid Surf. A* **682**, 132900 (2024).
79. Dong, S. et al. Flash Joule heating induced highly defective graphene towards ultrahigh lithium ion storage. *Chem. Eng. J.* **481**, 147988 (2024).
80. Xia, D. et al. Electrothermal transformations within graphene-based aerogels through high-temperature flash Joule heating. *J. Am. Chem. Soc.* **146**, 159–169 (2024).
81. You, L. et al. A graphene-like hollow sphere anode for lithium-ion batteries. *Chem. Commun.* **60**, 5030–5033 (2024).
82. Huang, J., Zhu, S., Zhang, J. & Han, G. One-pot ultrafast molten-salt synthesis of anthracite-based porous carbon for high-performance capacitive energy storage. *ACS Mater. Lett.* **6**, 2144–2152 (2024).
83. Ganjoo, R., Sharma, S., Kumar, A. & Daouda, M. M. A. in *Activated Carbon: Progress and Applications* (eds Verma, C. & Quraishi, M. A.) 1–22 (Royal Society of Chemistry, 2023).
84. Industrial Grade Multi Walled Carbon Nanotubes. *Nanografi* https://nanografi.com/carbon-nanotubes/industrial-grade-multi-walled-carbon-nanotubes-purity-92-outside-diameter-8-28-nm/?srsltid=AfmBOoqJyM625L7uy9AfazcwW97b4_PJ2Azm-SlEXgA8UXSRS8PFn8T-R (2024).
85. Multi Wall Carbon Nanotubes 99% Purity ~10-20nm. *Carb Lab Tech Supplies* https://www.carblabtechsupplies.com.au/product/multi-wall-carbon-nanotubes/2 (2024).
86. Advincula, P. A. et al. Tunable hybridized morphologies obtained through flash Joule heating of carbon nanotubes. *ACS Nano* **17**, 2506–2516 (2023).
87. Qin, G. et al. Millisecond activity modulation of atomically-dispersed Fe–N–C catalysts. *Energy Storage Mater* **69**, 103421 (2024).
88. Chen, J. et al. Boron nitride nanotube and nanosheet synthesis by flash Joule heating. Preprint at *ChemRxiv* https://doi.org/10.26434/chemrxiv-2024-mvrmf (2024).
89. Yuan, M., Yu, S., Wang, K., Mi, C. & Shen, L. Ultrafast synthesis of hard carbon for high-rate and low-temperature sodium-ion storage through flash Joule heating. *Solid. State Ion.* **414**, 116622 (2024).
90. Song, Z. et al. Joule heating for structure reconstruction of hard carbon with superior sodium ion storage performance. *Chem. Eng. J.* **496**, 154103 (2024).
91. Wang, L. et al. Rapid and up-scalable flash fabrication of graphitic carbon nanocages for robust potassium storage. *Adv. Funct. Mater.* **34**, 2401548 (2024).
92. Chen, W. et al. Millisecond conversion of metastable 2D materials by flash Joule heating. *ACS Nano* **15**, 1282–1290 (2021).
93. Aykol, M., Dwaraknath, S. S., Sun, W. & Persson, K. A. Thermodynamic limit for synthesis of metastable inorganic materials. *Sci. Adv.* **4**, eaaq0148 (2018).
94. Zhang, Y. et al. Direct observation of a widely tunable bandgap in bilayer graphene. *Nature* **459**, 820–823 (2009).
95. Liu, C. et al. Multiple twin boundary-regulated metastable Pd for ethanol oxidation reaction. *Adv. Energy Mater.* **12**, 2103505 (2022).
96. Liu, S. et al. Extreme environmental thermal shock induced dislocation-rich Pt nanoparticles boosting hydrogen evolution reaction. *Adv. Mater.* **34**, 2106973 (2022).
97. McHale, J. M., Auroux, A., Perrotta, A. J. & Navrotsky, A. Surface energies and thermodynamic phase stability in nanocrystalline aluminas. *Science* **277**, 788–791 (1997).
98. Klement, W., Willens, R. H. & Duwez, P. O. L. Non-crystalline structure in solidified gold–silicon alloys. *Nature* **187**, 869–870 (1960).
99. Grover, V., Mandal, B. P. & Tyagi, A. K. in *Handbook on Synthesis Strategies for Advanced Materials* Vol. I *Techniques and Fundamentals* (eds Tyagi, A. K. & Ningthoujam, R. S.) 1–49 (Springer Singapore, 2021).
100. Yu, M., Grasso, S., McKinnon, R., Saunders, T. & Reece, M. J. Review of flash sintering: materials, mechanisms and modelling. *Adv. Appl. Ceram.* **116**, 24–60 (2017).
101. Guillon, O. et al. Field-assisted sintering technology/spark plasma sintering: mechanisms, materials, and technology developments. *Adv. Eng. Mater.* **16**, 830–849 (2014).
102. Ping, W. et al. Printable, high-performance solid-state electrolyte films. *Sci. Adv.* **6**, eabc8641 (2020).
103. Chen, J. et al. Cathode interface construction by rapid sintering in solid-state batteries. *Small* **20**, 2307342 (2024).
104. Shin, J. et al. In_2Se_3 synthesized by the FWF method for neuromorphic computing *Adv. Electron. Mater.* https://doi.org/10.1002/aelm.202400603 (2024).
105. Yao, Y. et al. Carbothermal shock synthesis of high-entropy-alloy nanoparticles. *Science* **359**, 1489–1494 (2018).
106. Chen, Y. et al. Ultra-fast self-assembly and stabilization of reactive nanoparticles in reduced graphene oxide films. *Nat. Commun.* **7**, 12332 (2016).
107. Wang, M. et al. In situ generation of flash graphene supported spherical bismuth nanoparticles in less than 200 ms for highly selective carbon dioxide electroreduction. *ACS Mater. Lett.* **6**, 100–108 (2024).
108. Yu, F. et al. Rapid self-heating synthesis of Fe-based nanomaterial catalyst for advanced oxidation. *Nat. Commun.* **14**, 4975 (2023).
109. Luo, J. et al. Transient co-tuning of atomic Fe and nanoparticle facets for self-relaying Fenton-like catalysis. *Commun. Mater.* **5**, 9 (2024).
110. Yang, C. et al. Overcoming immiscibility toward bimetallic catalyst library. *Sci. Adv.* **6**, eaaz6844 (2020).
111. Liu, S. et al. Dislocation-strained IrNi alloy nanoparticles driven by thermal shock for the hydrogen evolution reaction. *Adv. Mater.* **32**, 2006034 (2020).
112. Li, P. et al. Flash joule heating synthesis of carbon supported ultrafine metallic heterostructures for high-performance overall water splitting. *J. Alloy. Compd.* **947**, 169630 (2023).
113. Qiu, Y. et al. Hybrid electrocatalyst Ag/Co/C via flash Joule heating for oxygen reduction reaction in alkaline media. *Chem. Eng. J.* **430**, 132769 (2022).
114. Xie, P. et al. Highly efficient decomposition of ammonia using high-entropy alloy catalysts. *Nat. Commun.* **10**, 4011 (2019).

115. Yao, Y. et al. Computationally aided, entropy-driven synthesis of highly efficient and durable multi-elemental alloy catalysts. *Sci. Adv.* **6**, eaaz0510 (2020).
116. Yao, Y. et al. High temperature shockwave stabilized single atoms. *Nat. Nanotechnol.* **14**, 851–857 (2019).
117. Zhu, W. et al. Ultrafast non-equilibrium synthesis of cathode materials for Li-ion batteries. *Adv. Mater.* **35**, 2208974 (2023).
118. Liao, Y. et al. Transient synthesis of carbon-supported high-entropy alloy sulfide nanoparticles via flash Joule heating for efficient electrocatalytic hydrogen evolution. *Nano Res.* **17**, 3379–3389 (2024).
119. Xia, D. et al. Flash Joule-heating synthesis of MoO nanocatalysts in graphene aerogel for deep catalytic oxidative desulfurization. *AIChE J.* **70**, e18357 (2024).
120. Wu, Y. et al. Roll-to-roll Joule-heating to construct ferromagnetic carbon fiber felt for superior electromagnetic interference shielding. *Carbon* **229**, 119474 (2024).
121. Qian, F. et al. Asymmetric active sites originate from high-entropy metal selenides by Joule heating to boost electrocatalytic water oxidation. *Joule* **8**, 2342–2356 (2024).
122. Dong, H. et al. Flash Joule heating: a promising method for preparing heterostructure catalysts to inhibit polysulfide shuttling in Li–S batteries. *Adv. Sci.* **11**, 2405351 (2024).
123. Huang, Z. et al. Direct observation of the formation and stabilization of metallic nanoparticles on carbon supports. *Nat. Commun.* **11**, 6373 (2020).
124. Song, J.-Y. et al. Generation of high-density nanoparticles in the carbothermal shock method. *Sci. Adv.* **7**, eabk2984 (2021).
125. Cui, M. et al. Multi-principal elemental intermetallic nanoparticles synthesized via a disorder-to-order transition. *Sci. Adv.* **8**, eabm4322 (2022).
126. Li, G. et al. Flash Joule heating to enhance water oxidation of hematite photoanode via mediating with an oxidized carbon overlayer. *Carbon* **215**, 118444 (2023).
127. Chen, Y. et al. SiC substrate/Pt nanoparticle/graphene nanosheet composite photocatalysts for hydrogen generation. *ACS Appl. Nano Mater.* **7**, 8958–8968 (2024).
128. Zhang, L. et al. Sub-second ultrafast yet programmable wet-chemical synthesis. *Nat. Commun.* **14**, 5015 (2023).
129. Deng, J. et al. Programmable wet-interfacial Joule heating to rapidly synthesize metastable protohematite photoanodes: metal and lattice oxygen dual sites for improving water oxidation. *ACS Catal.* **14**, 10635–10647 (2024).
130. Dong, Q. et al. Programmable heating and quenching for efficient thermochemical synthesis. *Nature* **605**, 470–476 (2022).
131. Lindberg, D., Molin, C. & Hupa, M. Thermal treatment of solid residues from WtE units: a review. *Waste Manag.* **37**, 82–94 (2015).
132. Chen, W. et al. Battery metal recycling by flash Joule heating. *Sci. Adv.* **9**, eadh5131 (2023).
133. Chen, W. et al. Flash recycling of graphite anodes. *Adv. Mater.* **35**, 2207303 (2023).
134. Lu, J. et al. Millisecond conversion of photovoltaic silicon waste to binder-free high silicon content nanowires electrodes. *Adv. Energy Mater.* **11**, 2102103 (2021).
135. Hao, J., Wang, Y., Wu, Y. & Guo, F. Metal recovery from waste printed circuit boards: a review for current status and perspectives. *Resour. Conserv. Recycl.* **157**, 104787 (2020).
136. Deng, B. et al. Flash separation of metals by electrothermal chlorination. *Nat. Chem. Eng.* **1**, 627–637 (2024).
137. Zhu, X.-H. et al. Recycling valuable metals from spent lithium-ion batteries using carbothermal shock method. *Angew. Chem. Int. Ed.* **62**, e202300074 (2023).
138. Wang, J. et al. Toward direct regeneration of spent lithium-ion batteries: a next-generation recycling method. *Chem. Rev.* **124**, 2839–2887 (2024).
139. Natarajan, S. & Aravindan, V. An urgent call to spent LIB recycling: whys and wherefores for graphite recovery. *Adv. Energy Mater.* **10**, 2002238 (2020).
140. Dong, S. et al. Ultra-fast, low-cost, and green regeneration of graphite anode using flash joule heating method. *EcoMat* **4**, e12212 (2022).
141. Ji, Y. et al. Regenerated graphite electrodes with reconstructed solid electrolyte interface and enclosed active lithium toward >100% initial coulombic efficiency. *Adv. Mater* **4**, e2312548 (2024).
142. Huang, P., Zhu, R., Zhang, X. & Zhang, W. A milliseconds flash Joule heating method for the regeneration of spent cathode carbon. *J. Environ. Sci. Health A* **57**, 33–44 (2022).
143. Yin, Y.-C. et al. Rapid, direct regeneration of spent $LiCoO_2$ cathodes for Li-ion batteries. *ACS Energy Lett.* **8**, 3005–3012 (2023).
144. Chen, W. et al. Nondestructive flash cathode recycling. *Nat. Commun.* **15**, 6250 (2024).
145. Lange, J.-P. Managing plastic waste — sorting, recycling, disposal, and product redesign. *ACS Sustain. Chem. Eng.* **9**, 15722–15738 (2021).
146. Wyss, K. M. et al. Converting plastic waste pyrolysis ash into flash graphene. *Carbon* **174**, 430–438 (2021).
147. Chen, Y. et al. Facilely preparing lignin-derived graphene–ferroferric oxide nanocomposites by flash Joule heating method. *Res. Chem. Intermed.* **49**, 589–601 (2023).
148. Khopade, K. V., Chikkali, S. H. & Barsu, N. Metal-catalyzed plastic depolymerization. *Cell Rep. Phys. Sci.* **4**, 101341 (2023).
149. Dong, Q. et al. Depolymerization of plastics by means of electrified spatiotemporal heating. *Nature* **616**, 488–494 (2023).
150. Selvam, E., Yu, K., Ngu, J., Najmi, S. & Vlachos, D. G. Recycling polyolefin plastic waste at short contact times via rapid Joule heating. *Nat. Commun.* **15**, 5662 (2024).
151. Amalina, F. et al. Biochar production techniques utilizing biomass waste-derived materials and environmental applications — a review. *J. Hazard. Mater. Adv.* **7**, 100134 (2022).
152. Jia, C. et al. Graphene environmental footprint greatly reduced when derived from biomass waste via flash Joule heating. *One Earth* **5**, 1394–1403 (2022).
153. Ding, D., Song, X., Wei, C. & LaChance, J. A review on the sustainability of thermal treatment for contaminated soils. *Environ. Pollut.* **253**, 449–463 (2019).
154. Gomez, E. et al. Thermal plasma technology for the treatment of wastes: a critical review. *J. Hazard. Mater.* **161**, 614–626 (2009).
155. Deng, B. et al. Heavy metal removal from coal fly ash for low carbon footprint cement. *Commun. Eng.* **2**, 13 (2023).
156. He, Z. et al. Ground-breaking and safe recycling of hazardous hyperaccumulators. *ACS EST. Eng.* **3**, 1966–1974 (2023).
157. Scotland, P. et al. Mineralization of captured per- and polyfluoroalkyl substances at zero net cost using flash Joule heating. Preprint at *ChemRxiv* https://doi.org/10.26434/chemrxiv-2023-6xj3m (2024).
158. McCleaf, P. et al. Removal efficiency of multiple poly- and perfluoroalkyl substances (PFASs) in drinking water using granular activated carbon (GAC) and anion exchange (AE) column tests. *Water Res.* **120**, 77–87 (2017).
159. Vargette, L. D. S. et al. Prospects of complete mineralization of per- and polyfluoroalkyl substances by thermal destruction methods. *Curr. Opin. Chem. Eng.* **42**, 100954 (2023).
160. Zhao, C., Dong, Y., Feng, Y., Li, Y. & Dong, Y. Thermal desorption for remediation of contaminated soil: a review. *Chemosphere* **221**, 841–855 (2019).
161. Luo, H., Zeng, Y., He, D. & Pan, X. Application of iron-based materials in heterogeneous advanced oxidation processes for wastewater treatment: a review. *Chem. Eng. J.* **407**, 127191 (2021).
162. Wu, X. et al. Joule heating-induced active Mg0 into nano-Mg composites for boosted oxidation and antiviral performance. *ACS EST. Eng*. https://doi.org/10.1021/acsestengg.3c00614 (2024).
163. Roberts, A. L., Totten, L. A., Arnold, W. A., Burris, D. R. & Campbell, T. J. Reductive elimination of chlorinated ethylenes by zero-valent metals. *Environ. Sci. Technol.* **30**, 2654–2659 (1996).
164. Sun, L. et al. Millisecond self-heating and quenching synthesis of Fe/carbon nanocomposite for superior reductive remediation. *Appl. Catal. B: Environ.* **342**, 123361 (2024).
165. Jia, C. et al. Joule heating induced reductive iron–magnesium bimetallic nanocomposite for eminent heavy metal removal. *ACS EST. Eng.* **4**, 938–946 (2024).
166. Wang, K. et al. Energy-efficient catalytic removal of formaldehyde enabled by precisely Joule-heated Ag/Co_3O_4@mesoporous-carbon monoliths. *Carbon* **167**, 709–717 (2020).
167. Du, P. et al. In-situ Joule-heating drives rapid and on-demand catalytic VOCs removal with ultralow energy consumption. *Nano Energy* **102**, 107725 (2022).
168. Zhang, L. et al. Size-controlled synthesis of graphene oxide sheets on a large scale using chemical exfoliation. *Carbon* **47**, 3365–3368 (2009).
169. Deng, B., Liu, Z. F. & Peng, H. L. Toward mass production of CVD graphene films. *Adv. Mater.* **31**, 1800996 (2019).
170. Lin, L., Deng, B., Sun, J. Y., Peng, H. L. & Liu, Z. F. Bridging the gap between reality and ideal in chemical vapor deposition growth of graphene. *Chem. Rev.* **118**, 9281–9343 (2018).
171. Cao, J. et al. Two-step electrochemical intercalation and oxidation of graphite for the mass production of graphene oxide. *J. Am. Chem. Soc.* **139**, 17446–17456 (2017).
172. Zink, T. & Geyer, R. Circular economy rebound. *J. Ind. Ecol.* **21**, 593–602 (2017).
173. Berkhout, P. H. G., Muskens, J. C. & W. Velthuijsen, J. Defining the rebound effect. *Energy Policy* **28**, 425–432 (2000).
174. Castro, C. G., Trevisan, A. H., Pigosso, D. C. A. & Mascarenhas, J. The rebound effect of circular economy: definitions, mechanisms and a research agenda. *J. Clean. Prod.* **345**, 131136 (2022).
175. Font Vivanco, D. et al. Rebound effect and sustainability science: a review. *J. Ind. Ecol.* **26**, 1543–1563 (2022).
176. Allan, G., Hanley, N., McGregor, P., Swales, K. & Turner, K. The impact of increased efficiency in the industrial use of energy: a computable general equilibrium analysis for the United Kingdom. *Energy Econ.* **29**, 779–798 (2007).
177. Han, Y.-C., Cao, P.-Y. & Tian, Z.-Q. Controllable synthesis of solid catalysts by high-temperature pulse. *Acc. Mater. Res.* **4**, 648–654 (2023).
178. Sahoo, P. K., Kim, K., Powell, M. A. & Equeenuddin, S. M. Recovery of metals and other beneficial products from coal fly ash: a sustainable approach for fly ash management. *Int. J. Coal Sci. Technol.* **3**, 267–283 (2016).
179. Furnaces and Boilers. *US Department of Energy* https://www.energy.gov/energysaver/furnaces-and-boilers (2024).
180. Jawad, S. K. Investigation of the dimensions design components for the rectangular indirect resistance electrical furnaces. *Am. J. Eng. Appl. Sci.* **3**, 350–354 (2010).
181. Xie, H. et al. Rapid liquid phase-assisted ultrahigh-temperature sintering of high-entropy ceramic composites. *Sci. Adv.* **8**, abn8241 (2022).
182. Fuel-fired furnaces and boilers (2022). *IPIECA* https://www.ipieca.org/resources/energy-efficiency-database/fuel-fired-furnaces-and-boilers-2022 (2022).
183. Reed, R. J. in *North American Combustion Handbook* Vol. 1, 3rd edn (North American Manufacturing Co., 1986).
184. Wei, W. et al. Thermally assisted liberation of concrete and aggregate recycling: comparison between microwave and conventional heating. *J, Mater. Civil. Eng.* **33**, 04021370 (2021).

Acknowledgements
Funding of the research is provided by the National Natural Science Foundation of China (no. 92475112, B.D.), the National Key R&D Program of China (2024YFC3907000, B.D.), the Air Force Office of Scientific Research (FA9550-22-1-0526, J.M.T.), the US Army Corps of Engineers, ERDC grants (W912HZ-21-2-0050 and W912HZ-24-2-0027, J.M.T.), the Defense Advanced Research Projects Agency (HR00112290122, J.M.T.) and the start-up funds of Tsinghua University (B.D.).

Author contributions
All authors made substantial contributions to the literature searching, writing, reviewing and editing of the manuscript. All aspects of the Review were overseen by J.M.T.

Competing interests
Some of the flash Joule heating processes and apparatus are the intellectual property of Rice University. B.D., L.E., K.M.W. and J.M.T. are listed as inventors on some issued patents or patent applications. The intellectual property of flash graphene synthesis has been licensed to Universal Matter Inc. and Universal Matter LLC. MTM Critical Metals and Flash Metals USA Inc. have licensed methods to remove metals from waste and ores. J.M.T. is a stockholder in these licensee companies, but he is not an officer, director or employee in the companies. All conflicts of interest are managed through regular disclosures to and compliance with Rice University's Office of Sponsored Programs and Research Compliance. K.M.W. is currently an employee of SLB. The authors declare no other competing interests.

Additional information
Supplementary information The online version contains supplementary material available at https://doi.org/10.1038/s44359-024-00002-4.

Peer review information *Nature Reviews Clean Technology* thanks Xiangdong Zhu; Micah Green, who co-reviewed with Ramu Banavath; and the other, anonymous, reviewer(s) for their contribution to the peer review of this work.